



Ollscoil Chathair
Bhaile Átha Cliath
Dublin City University

PS451 Final Year Project Report
**Accelerated Ageing of Novel Transparent
Conducting Oxides**

Name: Philip Keenan

Student No.: 16364523

Program of Study: BSc. in Applied Physics (AP4)

Supervisor: Dr. Karsten Fleischer

April 13, 2021

Declaration

Name: Philip Keenan

Student ID Number: 16364523

Programme: Applied Physics (AP4)

Module Code: PS451

Assignment Title: Final Year Project Report

Submission Date: 13 – APR – 2021

I understand that the University regards breaches of academic integrity and plagiarism as grave and serious.

I have read and understood the DCU Academic Integrity and Plagiarism Policy. I accept the penalties that may be imposed should I engage in practice or practices that breach this policy.

I have identified and included the source of all facts, ideas, opinions, viewpoints of others in the assignment references. Direct quotations, paraphrasing, discussion of ideas from books, journal articles, internet sources, module text, or any other source whatsoever are acknowledged and the sources cited are identified in the assignment references.

I declare that this material, which I now submit for assessment, is entirely my own work and has not been taken from the work of others save and to the extent that such work has been cited and acknowledged within the text of my work.

I have used the DCU library referencing guidelines (available at:
https://www.dcu.ie/library/classes_and_tutorials/citingreferencing.shtml) and/or the appropriate referencing system recommended in the assignment guidelines and/or programme documentation.

By signing this form or by submitting this material online I confirm that this assignment, or any part of it, has not been previously submitted by me or any other person for assessment on this or any other course of study.

By signing this form or by submitting material for assessment online I confirm that I have read and understood DCU Academic Integrity and Plagiarism Policy (available at:
<http://www.dcu.ie/registry/examinations/index.shtml>).

Name: Philip Keenan

Date: 13 – APR – 2021

Abstract

Transparent conducting oxide Indium-Tin-oxide thin films are used in many optoelectronic applications. However, due to the high cost and scarce availability of Indium, new transparent conductive oxides are being tested and developed to replace Indium Tin oxide. A leading transparent conducting oxide is Zinc oxide. However, Zinc oxide is known to be unstable in humid conditions while Indium-Tin oxide is not. Accelerated ageing techniques can show the level of conductivity and transparency of Zinc oxide after a number of years in a short period of time.

This project focuses on the accelerated ageing and comparison of amorphous Zinc-Tin oxide, Indium doped Zinc oxide and Indium and Aluminium co-doped Zinc oxide. These oxides were degraded through the use of the damp heat technique and their activation levels were calculated using an Arrhenius plot. It was found that the amorphous Zinc-Tin oxide is more stable in high-humidity environments than either doped Zinc oxide samples.

Acknowledgments

I would firstly like to thank my supervisor, Dr. Karsten Fleischer for giving me the opportunity to undertake this project. It was a privilege to work alongside him and add to his ongoing research in this exciting field.

His advice, and guidance throughout the year was vital to the successful completion of this project.

Many thanks also to Mr. Des Lavelle, there was no issue that he could not help with.

I would like to thank my family and friends for their love and support throughout my years in college, especially during the ongoing pandemic.

Finally, I would like to thank Patricija Pavelskopfa for her loving support throughout the last four years.

Contents

1	Introduction	1
1.1	Transparent Conducting Oxides	1
1.2	Indium Tin Oxide & Zinc Oxide	1
1.3	Long Term Degradation	1
1.4	Aims of Project	2
2	Theory & Background	3
2.1	Zinc Oxide	3
2.1.1	Stability in High Humidity Environment	3
2.2	Film Fabrication: Spray Pyrolysis	4
2.3	Damp Heat Technique	4
2.4	TCO Samples	6
2.4.1	Indium Doped Zinc Oxide	6
2.4.2	Indium & Aluminium co-doped Zinc Oxide	6
2.4.3	Amorphous ZTO-86 & ZTO-90	7
2.5	Activation Energy	9
2.6	Resistance Measurement	10
2.6.1	Circuit in Series	10
2.6.2	Two & Four Probe Methods	11
3	Experimental Methods	12
3.1	Resistance measurement device	12
3.1.1	Circuit Set Up	12
3.1.2	PCIe Card	13
3.1.3	LabView	14
3.1.4	Choosing applied voltage and known resistor	15
3.1.5	Ohmic properties of Device	15
3.1.6	Resistance measurement error	16
3.2	Heating Chamber & Clips	16
3.2.1	Heating Chamber	16
3.2.2	Sample Connection Clips	18
3.3	Sample Preparation	20
3.4	Moisture Test	21
3.4.1	Activation Levels	22
4	Results & Discussion	23
4.1	I-V Graph of device	23
4.1.1	Direct Connection	23
4.1.2	Connection Through Clips	24
4.2	Resistance Change	25
4.2.1	Nitrogen Flow	25
4.2.2	Oxygen Exposure	26
4.3	Accelerated Ageing Comparison	28
4.3.1	Sample ZnO:In	28
4.3.2	Sample ZnO:InAl	29
4.4	Activation Energy	30

5 Conclusions & Future Prospectives	34
5.1 Conclusions	34
5.2 Future Prospectives	34
5.3 A Brief note on Covid-19	35
References	36
A Appendix: Risk Assessment	38
B Arrhenius Plot Data	39
C LabView Program	40

List of Figures

Figure 2.1	Wurtzite crystal structure of ZnO at room pressure and temperature.	3
Figure 2.2	Schematic of Spray Pyrolysis.	4
Figure 2.3	Sheet Resistance of AZO for multiple RH levels.	5
Figure 2.4	Sheet Resistance of AZO for multiple temperatures.	5
Figure 2.5	Effect of substrate temperature on electrical properties of ZnO:In	6
Figure 2.6	Film composition and thickness vs relative molarity of ZTO-86 and ZTO-90. .	7
Figure 2.7	Renormalised transmission of samples ZTO-86 & ZTO-90.	8
Figure 2.8	Activation level requirement for a chemical reaction to take place.	9
Figure 2.9	Arrhenius plot of $\ln(k)$ versus 1/Temperature.	10
Figure 2.10	Schematic of four probe method apparatus.	11
Figure 3.1	Schematic of series circuit to obtain TCO resistance value.	12
Figure 3.2	Resistance measurement device - Breadboard and SCB-68 Pinout Board	13
Figure 3.3	Breadboard Schematic of circuit in series.	13
Figure 3.4	IV graph of an Ohmic device.	15
Figure 3.5	Heating Chamber and Heater Platform for DH experiments.	16
Figure 3.6	Water Supply of nebulizer attached to Heating Chamber.	17
Figure 3.7	Full system set up for a moisture test.	17
Figure 3.8	Multiple clips sizes used to measure resistance of TCO samples.	18
Figure 3.9	TCO sample secured to heater platform.	19
Figure 3.10	Notches cut into heating chamber for wires to clips.	19
Figure 3.11	Full TCO samples and cut sample sections.	20
Figure 3.12	LabView VI used to set up and run moisture tests.	22
Figure 4.1	I-V Graph of PCIe device with resistor connected in breadboard	23
Figure 4.2	I-V Graph of PCIe device with connection through clips	24
Figure 4.3	Resistance of TCO sample section at 70°C under Nitrogen flow.	25
Figure 4.4	Resistance of TCO sample section at 70°C exposed to Oxygen.	26
Figure 4.5	Round-trip tests of ZnO:In sample sections before and after moisture tests	28
Figure 4.6	Round-trip tests of ZnO:InAl sample sections.	29
Figure 4.7	Moisture test of ZnO:InAl sample at 200°C..	30
Figure 4.8	Moisture test of ZnO:InAl sample at 200°C after initial 500 seconds. . . .	30
Figure 4.9	Arrhenius plot for ZnO:InAl sample.	32
Figure 4.10	Arrhenius plot for all TCO samples.	32
Figure A.1	Risk assessment of lab project was carried out in.	38

List of Tables

Table 2.1	Resistivity value of ZnO thins films fabricated through different techniques. .	3
Table 2.2	Multiple ZnO:InAl thin films prepared through spray pyrolysis.	6
Table 3.1	Moisture test times.	21
Table 4.1	Resistance deviation under Nitrogen flow.	26
Table 4.2	Resistance deviation exposed to air.	27
Table 4.3	Average slope of ZnO:InAl sample for increasing temperatures.	31
Table 4.4	Activation energy of TCO samples.	33

1 Introduction

1.1 Transparent Conducting Oxides

Oxides are composed of at least one Oxygen atom and another element. In the case of Transparent Conducting Oxides (TCOs), the element is typically metallic, such as Zinc, Cadmium or Tin. [1] TCOs are electrical conductive materials whilst also being highly transparent in the solar spectrum. [2]

TCOs are better suited in many applications than other materials such as glass (insulator) and silicon and compound semiconductors (wavelength dependent optical resistors) since they can be fine tuned to alter their electrical conductivity and transparency. This is achieved through the use of semiconducting techniques. [2] A TCO can be doped with donor impurities or acceptor impurities that can affect important characteristics such as the electrical conductivity and transparency. [3]

1.2 Indium Tin Oxide & Zinc Oxide

TCOs are widely used in electronic devices due to their high levels of transparency and conductivity. Indium Tin oxide (ITO) is the most widely used TCO. However, Indium oxide is becoming scarce globally, proving to be expensive and difficult to obtain. [4] Due to this, new and improved TCOs are currently being developed and analysed in the hope to reduce cost and allow for new TCO devices to be made that ITO would hinder such as flexible displays. [5]

Many solar cells utilize TCOs as they allow for greater absorption of photons incident on the device while reducing internal series resistance. This increases the efficiency of the solar cell as more photons incident on the device are converted into electrical energy. [6] Solar cells become quite humid while being in direct sunlight. Certain TCOs such as Zinc oxide (ZnO) are known to be unstable in humid conditions under high irradiation levels.[4] This is problematic as ZnO is highly conductive, transparent and cost effective in relation to other TCOs. [7]

1.3 Long Term Degradation

Optoelectronic devices such as solar cells are exposed to heat and moisture on a daily basis as they are secured outside on roofs. While TCO thin films within these devices may experience large quantities of moisture from rain, they will not be exposed to temperatures high enough to quickly degrade them. They will however degrade slowly over a long period of time, excessive of 30 years. Due to this, it is important to understand how quickly a TCO thin film degrades and how well it will operate in 30 years time. Accelerated ageing can be used to achieve high levels of degradation similar to that experienced by a solar cell over 30 years.

Accelerated ageing consists of exposing TCO thin films to temperature and moisture levels higher than that experience in natural situations. This is done by heating TCO thin films to more than 100°C in an environment with relative humidity (RH) levels of more than 80%.

It is important to understand how TCO thin films degrade over long periods of time in high-relative humidity environments. As the electrical properties and cost of ZnO make it a promising candidate to replace ITO, a lot of research is being done to improve the stability of ZnO in high-relative humidity environments. This can be done through though the addition of impurities. Indium doped ZnO (ZnO:In) and Indium and Aluminium co-doped ZnO (ZnO:InAl) are examples of this. [8, 9] Amorphous Zinc Tin Oxide (ZTO) is also being examined. [10]

1.4 Aims of Project

This project is centred around the accelerated ageing and comparison of ZnO:In, ZnO:InAl and ZTO. Accelerated ageing will be achieved by using the damp heat (DH) technique while the change in resistance will be recorded in order to obtain the activation energy of each TCO sample. The aim of this project is to prove that ZTO is more stable in high humidity environments than ZnO:In and ZnO:InAl.

This project aims to develop a robust device capable of measuring the resistance change of the TCO samples during DH moisture tests. This device is expected to be functional within a heating chamber at temperatures up to 200°C and 100% RH level. This device will consist of a PCIe card, pinout board, breadboard and circuit in series. The device is to be programmed using LabView. This program and device will be integrated into a larger system used to fabricate, age and characterise TCO materials. The device can then be further developed and utilised for future experiments.

The TCO samples are to be placed in a heating chamber under constant Nitrogen flow, heated to temperatures up to 200°C and exposed to high levels of water vapour. By measuring the the change in resistance of the TCO samples during times when moisture is introduced into the chamber, an Arrhenius plot can be produced. This graph will all the activation energy of each sample to be calculated.

2 Theory & Background

2.1 Zinc Oxide

ZnO crystallizes in the wurtzite (B4 type) structure at room pressure and temperature as seen in Figure 2.1 below. [11] This hexagonal lattice is comprised of two interconnected hexagonal close packed (HCP) sub-lattices. These sub-lattices are Zn^{2+} and O^{2-} , meaning that each atom (either ZnO or O) is surrounded by the other atom in a tetrahedral shape. [11, 12] Due to this tetrahedral coordination, the structure is polar symmetric about the hexagonal axis. [11] This symmetric polarity is the cause of many properties of ZnO such as crystal growth and defect generation. [11]

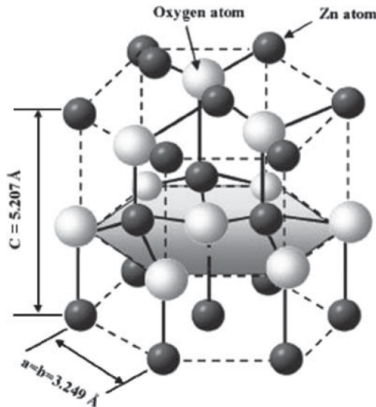


Figure 2.1: Wurtzite crystal structure of ZnO at room pressure and temperature. Taken from Reference [12].

ZnO at room temperature is an n-type semiconductor with a wide and direct band gap of 3.37eV that shows high transparency in the blue and near-UV spectral range. [3] The resistivity of ZnO has been shown to be in the range of $1 \times 10^{-3}\Omega\text{cm}$ to $8 \times 10^{-4}\Omega\text{cm}$ depending on the method of fabrication, as seen in Table 2.1 below. [13] These values are very similar to ITO and so, ZnO is an ideal replacement.

Fabrication Method	Resistivity (Ωcm)
Activated Reactive Evaporation	$\approx 8 \times 10^{-4}$
Magnetron Sputtering	$\approx 2 \times 10^{-3}$
Spray Pyrolysis	$\approx 10^{-3}$

Table 2.1: Resistivity values of ZnO fabricated using Activated Reactive Evaporation, Magnetron Sputtering and Spray Pyrolysis techniques. [13]

The values seen in Table 2.1 are highly dependent on solution concentrations and fabrication environment conditions. For instance, the ZnO fabricated through spray pyrolysis was annealed under H_2 at 350°C. A change in this temperature would result in a different resistivity value.

2.1.1 Stability in High Humidity Environment

While ZnO is an ideal replacement for ITO, it is known to be unstable in oxidizing environments. This is most noticeably seen in high temperature oxidizing environments which causes a rapid increase in resistivity. The stability of ZnO is highly dependent on the film deposition temperature. This means that films fabricated at high temperatures are less stable in oxidizing environments than films fabricated at lower temperatures. In order to use ZnO thin films in place of ITO thin films, stable ZnO films must be fabricated below 200°C. [4]

2.2 Film Fabrication: Spray Pyrolysis

Spray pyrolysis is a chemical deposition process (CDP) involving a precursor solution. This procedure has been used for mass production of large-area coatings of thin films. This technique involves a metal salt solution dissociated by pyrolytic decomposition into a metallic compound after it is sprayed onto a preheated substrate, seen in Figure 2.2 below. [14]

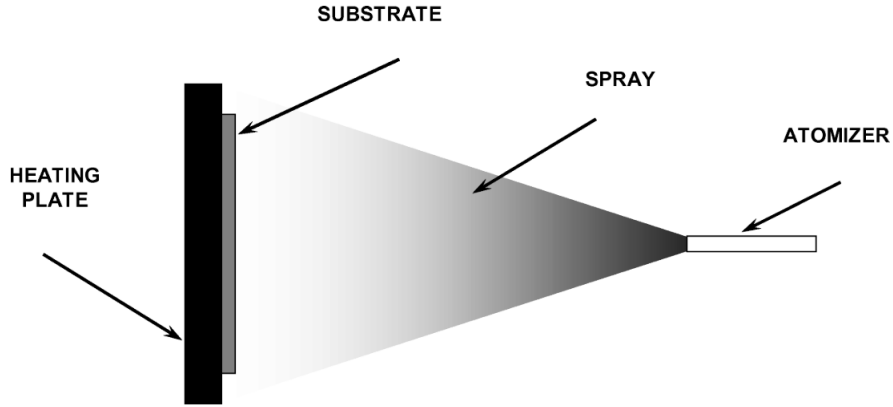


Figure 2.2: Schematic of Spray Pyrolysis. Taken from Reference [15]

Droplets from the spray spread into a disk shaped structure when they come into contact with the substrate. This results in a film composed of overlapping disk structures. The concentration of the spray mixture and the volume and momentum of the droplets influence the properties of the film produced, however the temperature of the substrate is the most critical parameter. [15]

2.3 Damp Heat Technique

The damp heat (DH) technique is used to accelerate the ageing of a TCO sample. The DH technique involves placing a TCO sample under heat and moisture levels that are considerably higher than levels experienced naturally.[16] By doing this, the TCO sample experiences a large amount of degradation in a short period of time. This gives an insight into the working condition of the TCO sample in the future. Degradation of a TCO results in an increase of resistance and a change of transparency level.[17]

To achieve sufficiently high levels of heat and humidity, chambers that allow for temperature and moisture control are used. TCO samples are placed into these chambers. Relative humidity (RH) is altered by pumping a stream of water-saturated air into the chamber.[16] Chambers are equipped with a heater to increase the temperature. The TCO sample can be placed directly on the heater to ensure the sample is as close to the desired temperature as possible. The stream of water-saturated air is directed onto the sample to ensure an even spread of moisture interacting with the sample.

A sufficiently high level of both heat and humidity is required for accelerated ageing to occur, and for the DH technique to be effective. This can be seen in Figure 2.3 below. The graph displays the change of sheet resistance of AZO at a constant temperature of 79°C with increasing RH over a long period of time.[16] A RH of 0.4% does not cause a change of resistance, meaning that degradation of the AZO sample did not take place. As the RH increases, a greater change of resistance is seen.

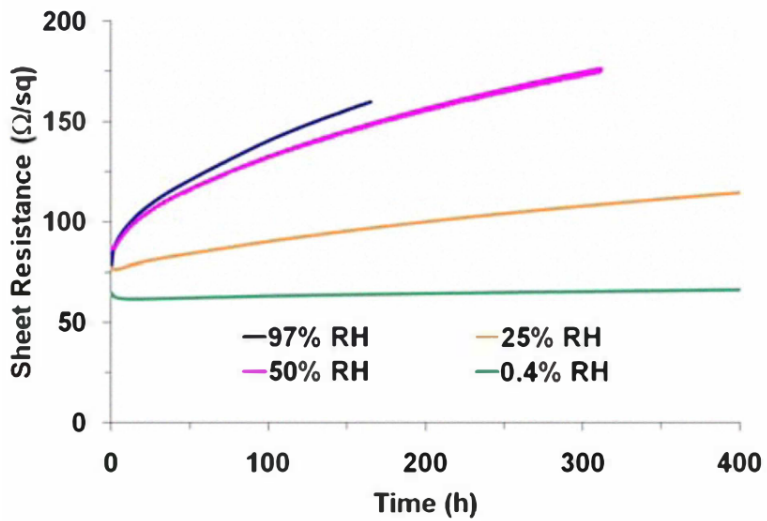


Figure 2.3: Sheet Resistance (Ω/sq) vs. Time(h) of AZO at 79°C for multiple RH levels. Taken from Reference [16]

The requirement for a sufficiently high temperature can be seen in Figure 2.4 below. The graph displays the change of sheet resistance of AZO at a constant RH of 85% with increasing temperature over a long period of time.[16] Below 50°C, little to no resistance change can be seen while at 85°C, a dramatic change in resistance is observed.

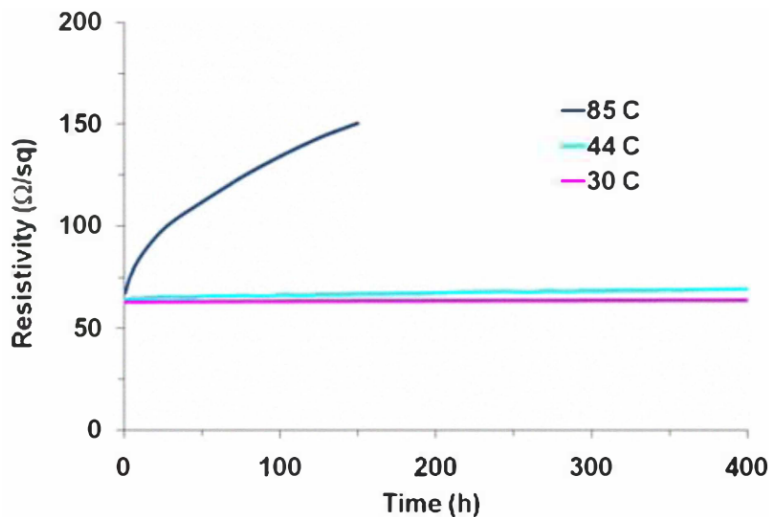


Figure 2.4: Sheet Resistance (Ω/sq) vs. Time(h) of AZO at 85% RH for multiple temperatures. Taken from Reference [16]

2.4 TCO Samples

The TCO samples examined in this project are Indium doped Zinc oxide (ZnO:In), Indium and Aluminium co-doped Zinc oxide (ZnO:InAl) and amorphous Zinc-Tin oxide (ZTO).

2.4.1 Indium Doped Zinc Oxide

The ZnO:In sample was fabricated using spray pyrolysis. The temperature at which a ZnO:In thin film is grown drastically changes the electrical properties. This can be seen in Figure 2.5 below. For thin films grown between 380°C and 450°C, electrical resistivity initial decreases as the growing temperature increases and reaches a minimum of $7.3 \times 10^{-3} \Omega\text{cm}$ at 415°C before steadily increasing. Carrier mobility and carrier concentration can also be seen to change with respect to temperature. [8]

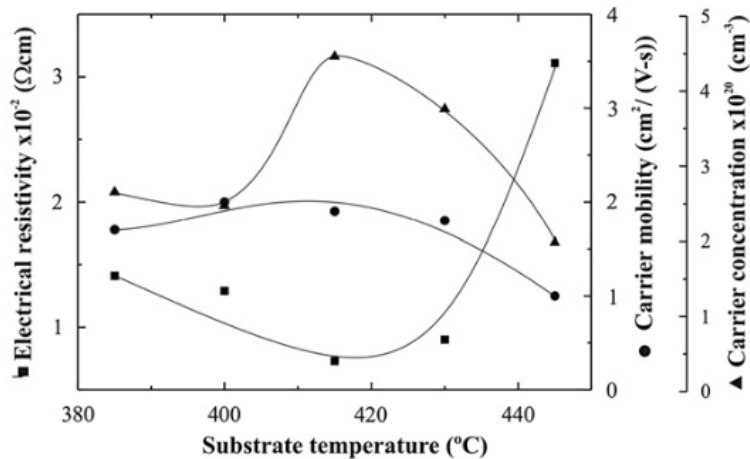


Figure 2.5: Effect of substrate temperature on electrical resistivity, carrier mobility and carrier concentration of ZnO:In. Taken from Reference [8]

2.4.2 Indium & Aluminium co-doped Zinc Oxide

The ZnO:InAl sample was fabricated using spray pyrolysis. The precursors used and doping concentration change electrical properties of ZnO:InAl samples. Table 2.2 below displays a number of ZnO:InAl thin films with a range of Al and In concentrations and their corresponding resistivity values. Both precursor types (ALCL & ALS) had a molarity of 0.1M. ALCL was a precursor of Aluminium Chloride dissolved in Methanol and ALS was a precursor of Aluminium Sulphate dissolved in Methanol.

Thin Film ID	Al Precursor	Al concentration (at%)	In concentration (at%)	Resistivity Ωcm
ALCL-1	ALCL	1	1	5.45×10^{-3}
ALCL-2	ALCL	2	2	3.44×10^{-3}
ALCL-3	ALCL	3	3	7.00×10^{-3}
ALS-1	ALS	1	1	5.49×10^{-3}
ALS-2	ALS	2	2	7.39×10^{-3}
ALS-3	ALS	3	3	8.18×10^{-3}

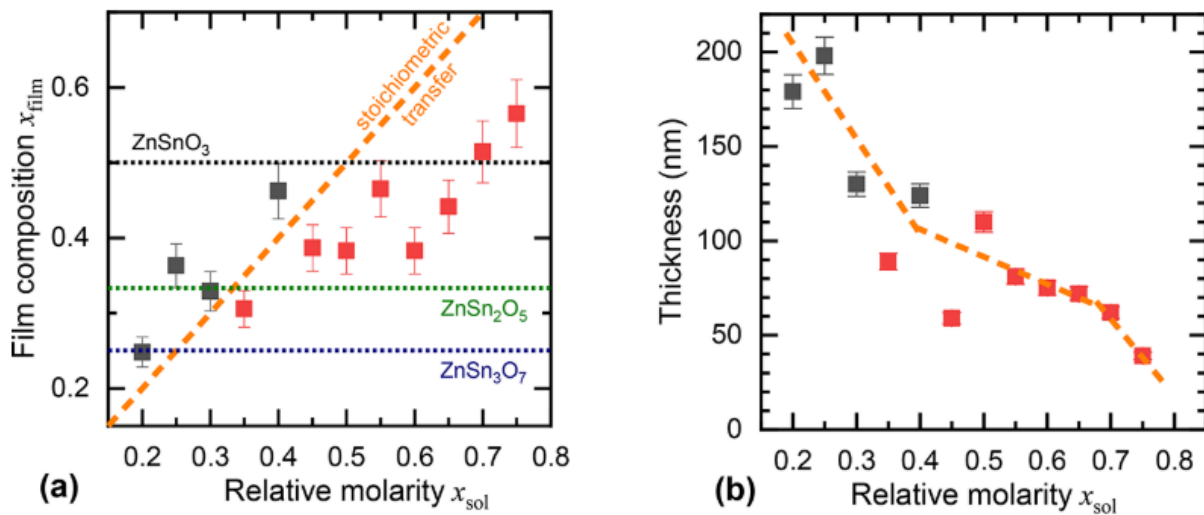
Table 2.2: ZnO:InAl thin films prepared through spray pyrolysis with a range of Al and In concentrations and their corresponding resistivity values. [9]

From Table 2.2 above, it is clear that the correct precursors and dopant concentration is vital in order to produce thin films with low resistivity.

2.4.3 Amorphous ZTO-86 & ZTO-90

Both amorphous ZTO samples were grown using spray pyrolysis. The samples were grown at 450°C for 900s in a chamber with gas composition of 95% Nitrogen and 5% Oxygen. The precursors used were a mixture of Zinc Chloride (ZnCl_2) and tin-diethylhexanonate dissolved in methanol. Total molarity of the precursors was 0.05M. [18]

The Zn:Sn precursor ratio was 65:35 and 50:50 for ZTO-86 and ZTO-90, respectively. Once the samples were grown, the Zn:Sn ratio was roughly 60:40 for both. Figure 2.6a below displays the film composition against relative molarity of Zn for a range of Zn:Sn ratios. It can be seen that Zn:Sn ratios around 50:50 result in a similar film composition. The two centre dots beside each other are the ZTO-86 and ZTO-90 samples. [18]



(a) Film composition vs. relative molarity. ZTO-86 and ZTO-90 are the two centre red markers.
(b) Film Thickness vs. relative molarity of ZTO-86 and ZTO-90.

Figure 2.6: Film composition and thickness vs relative molarity of ZTO-86 and ZTO-90. Taken from Reference [18]

Figure 2.6b above displays the film thickness against relative molarity of Zn for a range of Zn:Sn ratios. The film thickness of ZTO-86 is 72nm and 110nm for ZTO-90.

Figure 2.7 below displays a graph of renormalised transmission for both ZTO-86 and ZTO-90. These samples are highly transparent in the visible and infrared light ranges. [18]

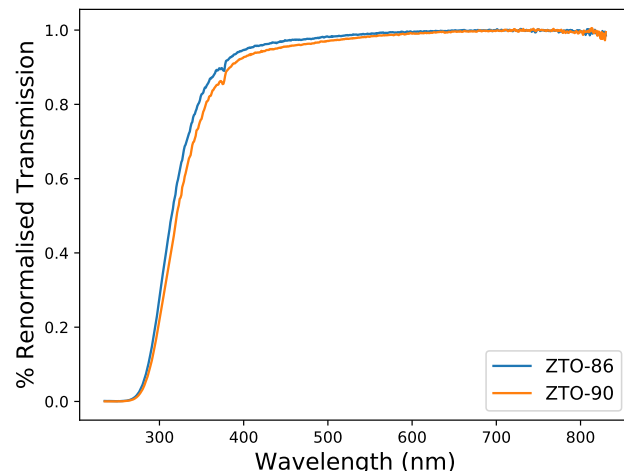


Figure 2.7: Renormalised transmission of samples ZTO-86 & ZTO-90. Data was provided by Dr. Karsten Fleischer as part of on-going research.

As both samples have a Zn:Sn film composition ratio of 60:40, there is significantly less ZnO than in the doped ZnO samples. Due to this, it would be expected that the amorphous ZTO samples are more stable in high-humidity environments than the doped samples.

2.5 Activation Energy

The activation energy (E_a) of a material is the minimum energy required by a molecule for a chemical reaction to occur. [19] The molecule requires enough kinetic or potential energy to break their chemical bonds. The higher the activation energy, the harder it is for molecules to break their chemical bonds.

Figure 2.8 displays the activation energy required for a chemical reaction to occur. The reactants within the material that obtain sufficient energy can reach the transition state where a reaction takes place.

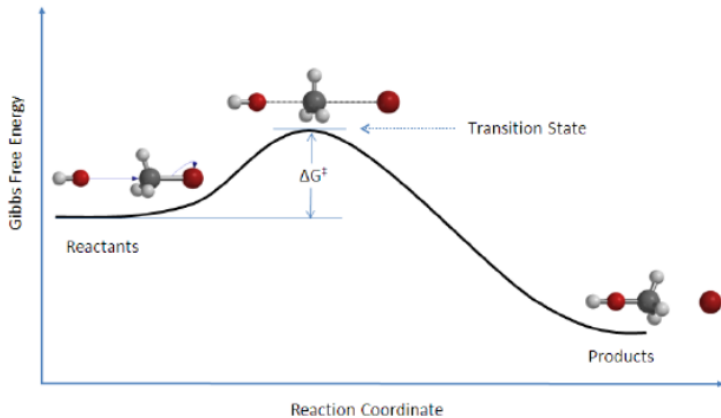


Figure 2.8: Activation level requirement for a chemical reaction to take place. Taken from Reference [19]

To obtain the activation energy of a material, the Arrhenius equation is used, seen in Equation 1 below. This equation relates the activation energy of a material with the rate constant. As the temperature of a material increases, more molecules have sufficient energy to overcome the energy barrier and reach the transition state seen in Figure 2.8 above. The fraction of molecules with energy greater or equal to the activation energy is given by $\exp(-\frac{E_a}{RT})$.

$$k = Ae^{-E_a/RT} \quad (1)$$

In Equation 1 above, k is the rate constant, E_a is the activation energy, R is the gas constant (8.3145 J/mol/K), T is temperature in Kelvin and A is the Arrhenius factor.

$$\ln(k) = -\frac{E_a}{R}[\frac{1}{T}] + \ln(A) \quad (2)$$

$$y = m.x + c \quad (3)$$

By obtaining the natural log of both sides of Equation 1 above, one can arrive at Equation 2. Equation 2 resembles the equation of a straight line seen in Equation 3.

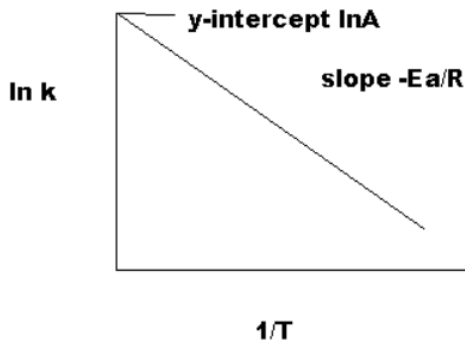


Figure 2.9: Arrhenius plot of $\ln(k)$ versus $1/\text{Temperature}$. Taken from Reference [19].

By obtaining a graph of $\ln(k)$ versus $1/\text{Temperature}$, such as in Figure 2.9 above, a straight line with a slope of $-\frac{E_a}{R}$ and a y-intercept of $\ln(A)$. The activation energy of a material can be calculated by obtaining the slope from a $\ln(k)$ versus $1/\text{Temperature}$ graph and multiplying it by $-R$, as in Equation 4 below.

$$E_a = -R.\text{Slope} \quad (4)$$

For a graph of $\ln(k)$ versus $1/\text{Temperature}$, a reaction with a higher E_a results in a straight line with a steeper slope than a reaction with a lower E_a . This means that a reaction rate with a higher E_a is very sensitive to temperature change.

2.6 Resistance Measurement

2.6.1 Circuit in Series

A circuit at constant temperature with Ohmic components obeys Ohms law, equation 5 below. In equation 5, V is the applied voltage, I is current flow and R is resistance. Components of a circuit may be connected in series or in parallel. This project utilizes a circuit in series.

$$V = IR \quad (5)$$

Within a circuit in series, the total voltage across the circuit is the sum of the voltage drops across each component in the circuit. The current across each component in a circuit in series is equal. The total resistance of the circuit is the sum of all resistances in the circuit, as seen in equation 6 below.

$$R_{\text{Total}} = R_1 + R_2 + \dots + R_n \quad (6)$$

Ohms law can be applied to each individual component of a circuit in series. By knowing the resistance value of a component and being capable of measuring the voltage drop across the component, one can calculate the current across the entire circuit. This value may then be used to calculate the resistance or voltage drop of other components in the circuit, depending on other known values.

2.6.2 Two & Four Probe Methods

Two and four probe methods can be used to measure the surface resistivity of a material. The two probe method consists of measuring a potential difference between two probes placed a small distance from each other on the material. The four point probe method uses a piece of equipment with four probes arranged in a straight line, as seen in Figure 2.10 below. A constant current is passed through the two outer probes and a voltage drop is measured across the middle probes. [20]

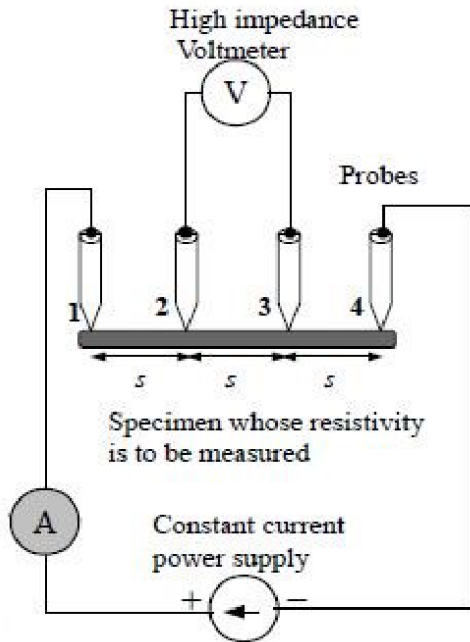


Figure 2.10: Schematic of four probe method apparatus. Taken from Reference [20]

The four probe method is superior than the two probe method. This is due to the two probe method being unable to separate the measured resistivity, including the resistivity due to the probes, and the resistivity of the material being tested. [21]

3 Experimental Methods

3.1 Resistance measurement device

To conduct experiments in which the change in resistance of a TCO sample is recorded, I was required to construct and program an instrument capable of doing this. The device was constructed using a PCIe-6024e card, SCB-68 pinout board and breadboard. A circuit in series was constructed between the pinout board and breadboard. LabView version 8.5 was used to program the device and the DAQmx extension was utilized for communicating with the device.

3.1.1 Circuit Set Up

To measure a change of resistance, the TCO sample was placed in series with a known resistor in order to utilize the electronic properties of resistors in series, as discussed in Section 2.6.1. This circuit can be seen in the schematic Figure 3.1 below. The circuit was comprised of an applied voltage, a known resistor and an unknown resistor, the TCO sample, in series. A voltage drop was measured across each of these components.

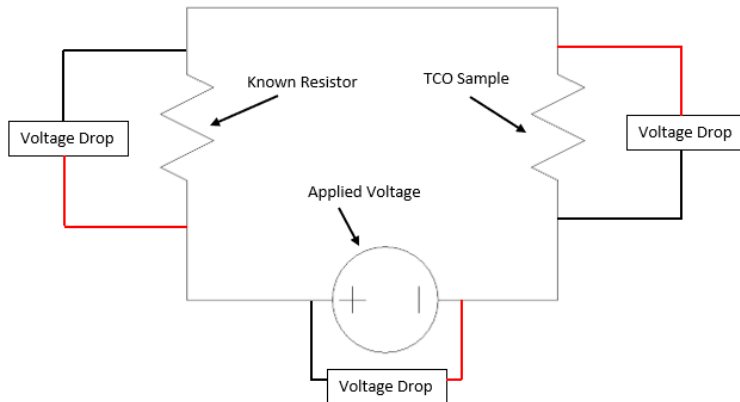


Figure 3.1: Schematic of series circuit to obtain TCO resistance value.

To obtain the resistance value of the TCO sample, the current in the circuit was calculated. This was done by measuring the voltage drop across the known resistor, the value of the resistor which is known and rearranging Ohms law, equation 5 above.

Due to the known resistor and TCO sample being in series, the current was constant throughout the circuit and therefore, could be used to calculate the TCO sample resistance value. The resistance of the TCO sample was calculated using the current and voltage drop across the TCO sample, as seen in equation 7 below.

$$R_x = \frac{V_x}{I} \quad (7)$$

In equation 7 above, R_x and V_x are the resistance value and voltage drop of the TCO sample, respectively. This equation can be expanded to equation 8 below. This includes the method by which the current value was obtain, R_K and V_K are the resistance value and voltage drop of the known resistor, respectively.

$$R_x = \frac{V_x R_K}{V_K} \quad (8)$$

3.1.2 PCIe Card

The voltage drop across the known resistor and TCO sample were measured using a PCIe-6024e card. This card also supplied the voltage across the circuit. A SCB-68 pinout board was utilized to make connections between the circuit, constructed on a breadboard, and PCIe card, as seen in Figure 3.2 below.

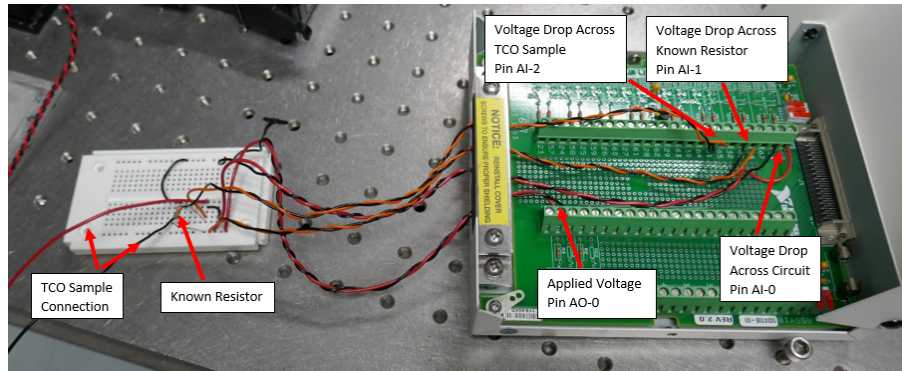


Figure 3.2: Resistance measurement device - Breadboard and SCB-68 Pinout Board

Each pin of the PCIe card had a corresponding ground pin that was utilized to create a closed circuit when a pin was used. The PCIe card supplied a voltage across the circuit through output pin AO-0. The applied voltage value could be changed. The input pins AI-1 and AI-2 measured the voltage drop across the known resistor and TCO sample, respectively. The AI-0 input pin measured the voltage drop across the entire circuit to insure the voltage being supplied was constant and equal to the selected value in the LabView program. The wiring of connections on the breadboard can be seen in Figure 3.3 below.

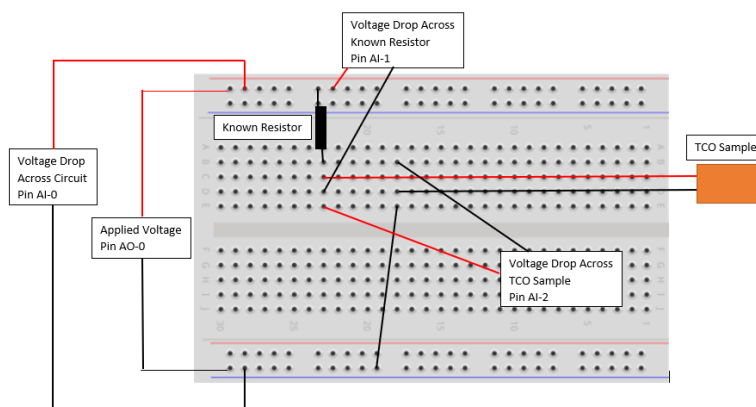


Figure 3.3: Breadboard Schematic of circuit in series.

3.1.3 LabView

The output and inputs of the PCIe card were controlled and read using LabView software. The DAQmx extension was used as it includes functions capable of controlling and working with the PCIe card. Two virtual instruments (VIs) were created using this software to output a desired applied voltage and read the values of the voltage drops from the three inputs, respectively. These programs can be found in Appendix C below.

The DAQmx functions 'Create Virtual Channel', 'Read', 'Stop Task' and 'Clear Task' were used to create a VI capable of measuring the voltage drops across the known resistor, TCO sample and entire circuit. The 'Create Virtual Channel' was set to 'AI Voltage'. This was capable of reading voltages. The channels to be read were also set as part of this function. They were 'Card/ai0', 'Card/ai1' and 'Card/ai2'. These correspond to the input pins of the PCIe card discussed in Section 3.1.2 above. 'Card' was the name set for the PCIe card in order to distinguish it from other devices that use DAQmx.

The 'Read' function was set to read N analog channels, at one sample per channel. It returned all three channel values in an array. The 'Index Array' function was used to split this array into the three individual elements. The first element, corresponding to AI-0, was the voltage drop across the full circuit. The second element, corresponding to AI-1, was the voltage drop across the known resistor. The value of the known resistor was set manually in the program and was used along with this voltage drop measurement to determine the value of the current flow in the circuit, as discussed in Section 2.6.1 above. The third element, corresponding to AI-2, was the voltage drop across the TCO sample. The value of the current in the circuit and this voltage drop was used to calculate the resistance value of the TCO sample.

The functions 'Stop Task' and 'Clear Task' were used to cease the program. This ensured that the program was not executing when it was not being called and released any resources that were used. This allowed other programs to use these resources.

The VI created to output a voltage across the circuit also used the 'Create Virtual Channel', 'Stop Task' and 'Clear Task' functions. In this case, the 'Create Virtual Channel' was set to 'AO Voltage', capable of outputting a voltage. The channel selected was 'Card/ao0', corresponding to AO-0. The 'Write' function was used instead of the 'Read' function in order to output a voltage.

These VIs were integrated into an existing VI that was used to control the heating module that the TCO samples were placed into. This VI had been developed and improved for 10 years and had a lot of functionality that this project benefited from. The VI was set up to save data, select specific time ranges for tests and set the temperature of heating module. The two VIs created for this project had the possibility of possessing this functionality. However, to do so was beyond the time frame of this project. It was also always intended for the device discussed here to be integrated into the heating module set up for further use after this project has concluded.

3.1.4 Choosing applied voltage and known resistor

The applied voltage across the circuit and known resistor value were the only components of the circuit that could be changed manually and controlled. Due to this, it was important that the ideal value of each was used to reduce noise within the circuit in order to obtain useful data.

The initial known resistor used while the device was under development was 100Ω . The resistance values of the TCO samples were in the range of 600Ω - $1.7k\Omega$. This meant that as the resistance of the TCO sample increased during moisture tests, the voltage drop across the sample would also increase. This would result in a decrease of voltage drop across the known resistor and would affect the accuracy of the current flow calculation. To reduce this inaccuracy, the known resistor was changed to 510Ω as it caused the difference between the known resistor voltage drop and the TCO sample voltage drop to remain small.

To determine the ideal applied voltage, values from $1V$ - $5V$ were used to obtain the value of a known resistor in place of the TCO sample. A range of resistor values were used for both the known and unknown resistors. Resistance measurements at constant temperature were ran for 2 minutes. The maximum and minimum resistance were recorded. These values and the difference between them were compared to the actual value of the resistor in place for the TCO sample. An applied voltage of $3V$ was deemed to be ideal as it resulted in the smallest difference between the maximum and minimum resistance values for majority of the known and unknown resistor combinations.

3.1.5 Ohmic properties of Device

The moisture tests carried out on the TCO samples were completed at constant temperatures. There was a change in resistance during the test, which implied a non-Ohmic interaction was occurring. To ensure that the TCO sample was the reason for this non-Ohmic interaction, and not the fabricated device or the clips used to make a connection with the sample, two IV curves were created.

For the device to be considered Ohmic, the IV curve should be a straight line through the origin, as seen in Figure 3.4 below. By rearranging equation 5, Ohms Law, it can be said that resistance is voltage over current. This means that the inverse of the slope seen in Figure 3.4 is the resistance of the device.

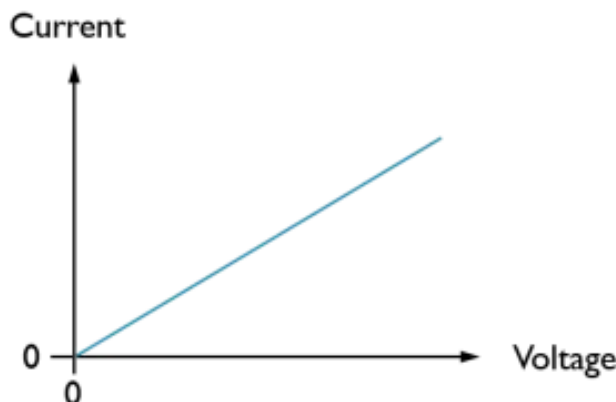


Figure 3.4: IV graph of an Ohmic device displaying a straight line through the origin. The resistance of the device is $1/\text{slope}$.

The current and voltage of the device were recorded from 0 - 5V in steps of 0.1V. There was a slight difference between the selected voltage value and the value measured by input AI-0. The measured voltage value was used to create the IV curves. For the first IV curve, a known resistor was connected into the breadboard in place of the clips that connect to TCO sample. The second IV curve had the known resistor connected through the clips. This known resistor was $1.49\text{k}\Omega$. The total resistance of the circuit was $2\text{k}\Omega$.

3.1.6 Resistance measurement error

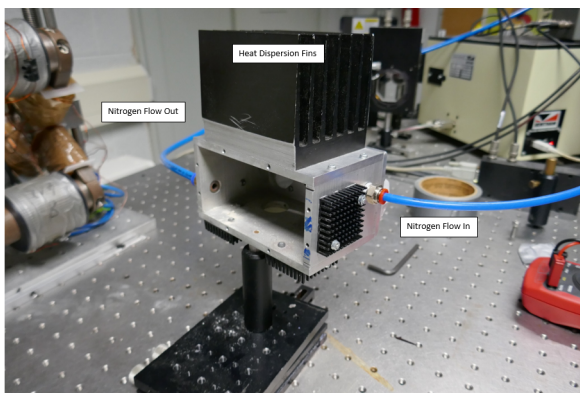
When a TCO sample is not exposed to moisture and it is at a constant temperature, there should be no fluctuation in resistance value. To illustrate that there is indeed a change in resistance under these conditions, a graph of resistance vs temperature at 70°C was created. The test was carried out twice, both for a duration of 20 minutes. The first test was completed under nitrogen flow and the second was completed with the heating chamber open, without nitrogen flow. This was also done to show that the resistance fluctuation is similar with and without nitrogen flow.

3.2 Heating Chamber & Clips

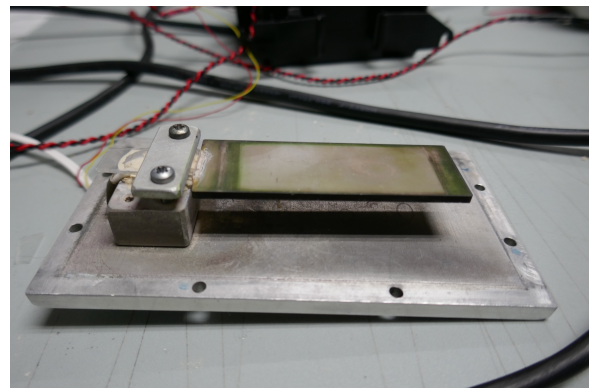
3.2.1 Heating Chamber

TCO samples were placed into the chamber seen in Figure 3.5a below. Heat and moisture conditions were controllable within this chamber. Figure 3.5b displays the heater that the TCO sample is placed onto. This allowed the temperature of the sample to be changed to desired temperatures. For this project, the range of temperatures that the samples were examined under was between 60°C and 200°C . The temperature of the heater was controlled by a temperature sensor through a LabView VI. This sensor also recorded the temperature when requested and can be seen in Figure 3.7 below.

The TCO samples were placed on the heater and secured by clips to be discussed in Section 3.2.2. The heater was screwed to the opening of the chamber, this closed the heating chamber. In order to reduce Oxygen interactions with the samples, the chamber was under constant Nitrogen flow. The blue tubes in Figure 3.5a supplied Nitrogen in (right tube) and out (left tube).



(a) Heating Chamber with Nitrogen Tubes attached.



(b) Heater Platform

Figure 3.5: Heating Chamber and Heater Platform for DH experiments.

Moisture within the chamber was controlled using a nebulizer machine. When this was turned

on, water vapour was pumped into the chamber through the opening seen in Figure 3.6 below. The nebulizer was turned on at specific intervals. Once the nebulizer was switched off, the Nitrogen flow would remove the water vapour from the chamber. When moisture tests were not being carried out, the water container was unattached from the chamber and the opening was sealed with duct tape.

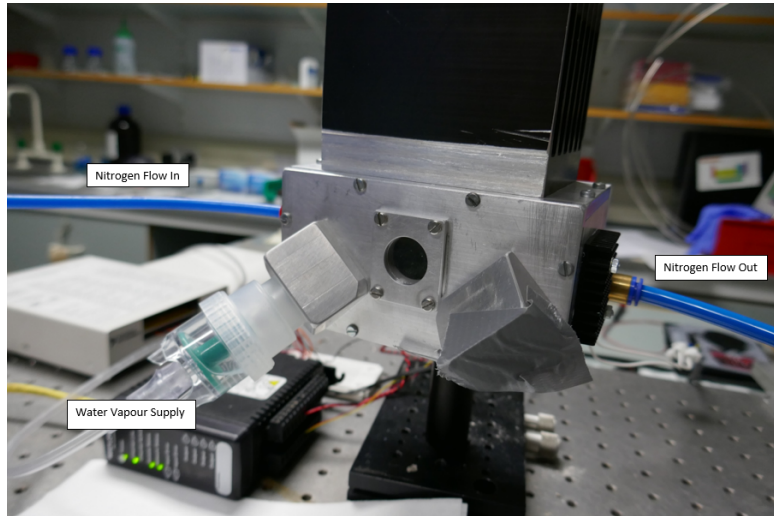


Figure 3.6: Water Supply of nebulizer attached to Heating Chamber.

The full system can be seen in Figure 3.7 below. The power supply was connected to the temperature sensor in order to control the heater within the chamber. Once the system was set up and an experiment was being carried out at a specific temperature, all measurements were made automatically and the temperature was maintained by the heater. The nebulizer was the only manual instrument in this set up.

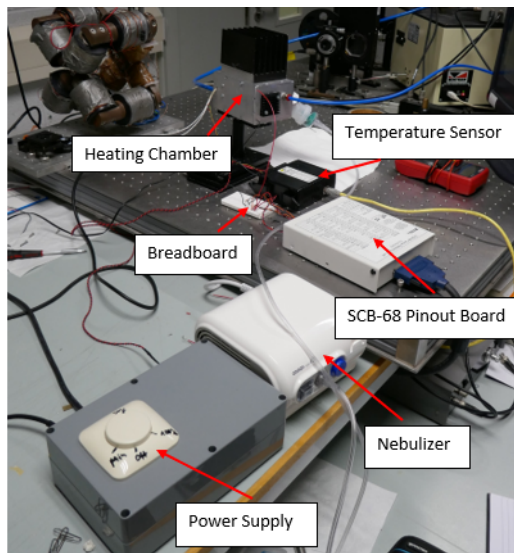


Figure 3.7: Full system set up for a moisture test.

3.2.2 Sample Connection Clips

Specialised clips were required to be fabricated in order to measure the resistance change of a TCO sample in the heating chamber. To ensure a connection was made from one clip, through the TCO sample and to the second clip, a clip with a large surface area was required. The design used to make these clips was a 'U' shape with a screw underneath and a screw on the back, as seen in Figure 3.8a below. The screw underneath was used to secure the clip and TCO sample to the heater while the screw on the back was used to make a connection to the breadboard and circuit in series. The clips were fabricated using Aluminium to ensure minimal loss in the resistance measurement of the TCO sample.

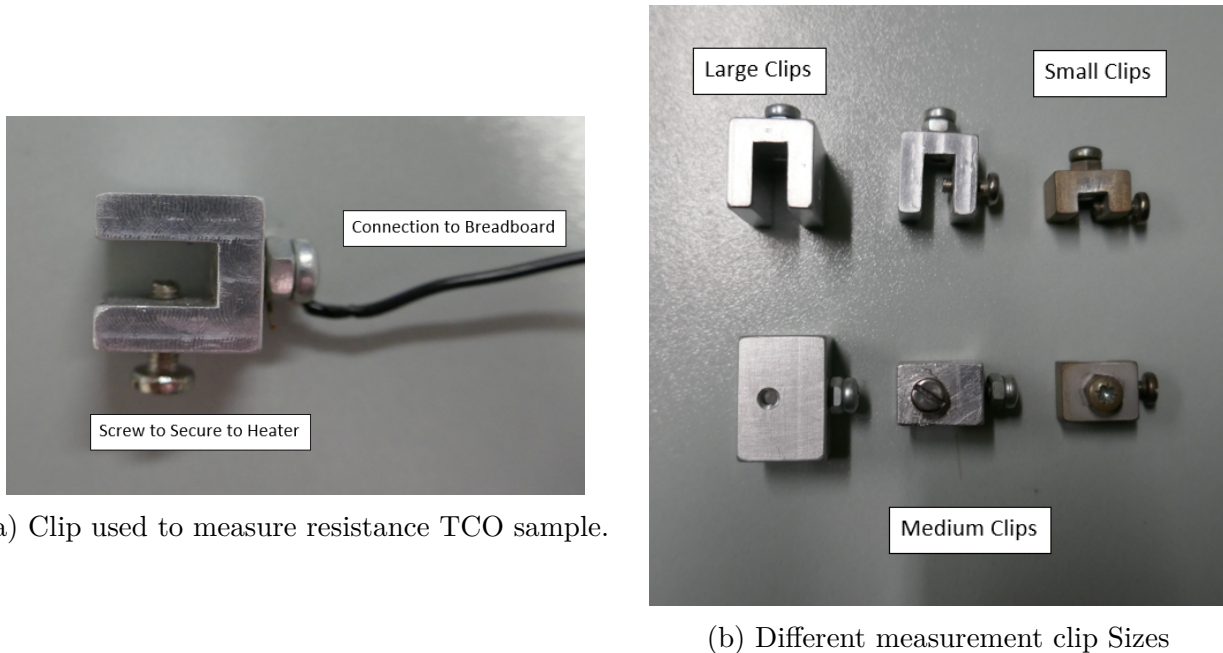


Figure 3.8: Multiple clips sizes used to measure resistance of TCO samples.

The first version of these clips are the large clips seen in Figure 3.8b above. The surface area of these were found to be too big as the resistance values recorded had a large error margin. The large clips were cut in half to produce the medium clips in Figure 3.8b above. These clips were used for the remainder of the project. The small clips seen in Figure 3.8b above were also fabricated to allow a larger distance across the TCO sample to be measured. These clips were not used during this project.

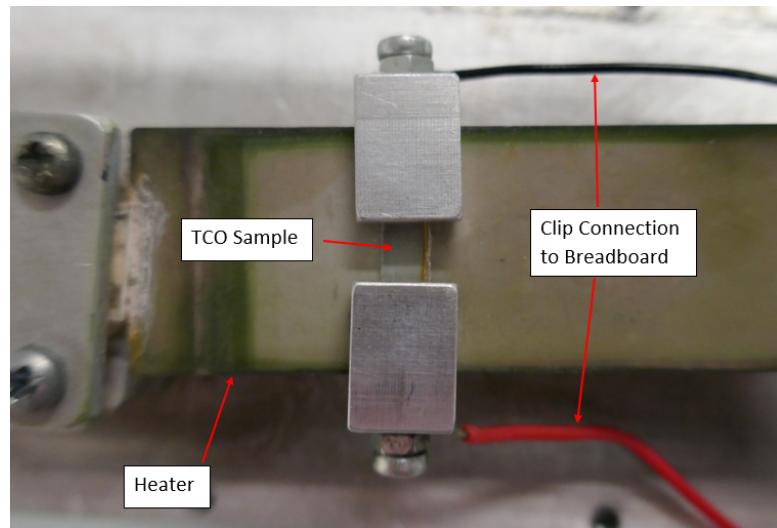


Figure 3.9: TCO sample secured to heater platform.

To ensure the heater chamber was securely sealed, two notches were cut into the side wall of the chamber, as seen in Figure 3.10 below. These allow the two wires connected to the clips to be connected to the breadboard without creating a leak in the chamber.

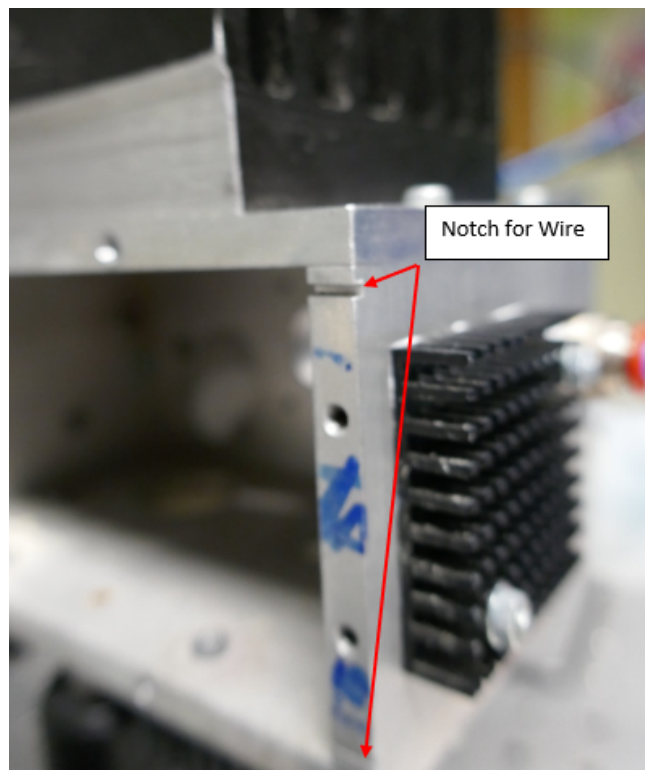


Figure 3.10: Notches cut into heating chamber for wires to clips.

3.3 Sample Preparation

The TCO samples examined during this project were ZnO:InAl, ZnO:Al and ZTO, as discussed in Section 2.2 above. Al TCO samples were tested under multiple heat and moisture conditions. To achieve this, The full samples were cut into individual sample sections roughly 7cm in width. A full sample and individually cut samples sections can be seen in Figure 3.11 below.

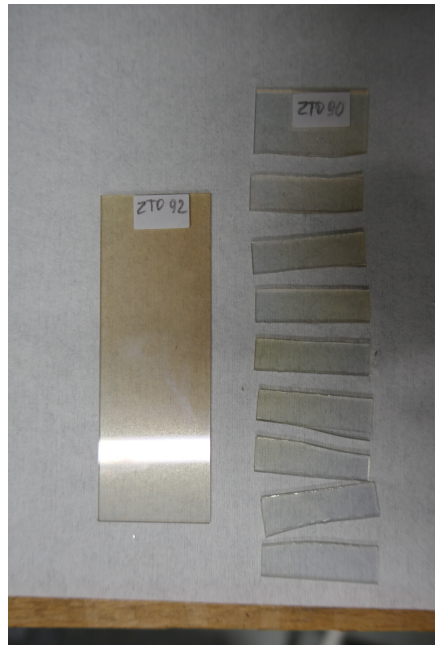


Figure 3.11: Full TCO samples and cut sample sections.

Some of the samples had been fabricated a number of months before this project under Nitrogen flow. Impurities such as Oxygen may have come in contact with the samples between fabrication and testing. This would alter the condition and results recorded from moisture tests. To remove these impurities prior to moisture tests, the samples were annealed under Nitrogen flow at 120°C for 10 minutes. While this process does not restore the samples to their original working condition immediately following their fabrication, it does improve their electrical properties and ensures that they were in the best working condition as possible.

The working condition of a sample was examined before a moisture test was carried out. This was achieved by measuring the resistance of the oxide while heating the sample in the heating chamber from 50°C to 150°C and back to 50°C under Nitrogen flow. This test was repeated after the moisture test of a sample and compared to the first test in order to examine the change in working condition of the sample.

3.4 Moisture Test

Moisture tests were carried out to examine how TCO samples degrade using the DH technique. This was completed by recording the resistance change of a TCO sample while it was subject to moisture in the form of water vapour and heated to constant temperatures by the heater. From these measurements, it was possible to obtain the activation energy of the different TCO samples using an Arrhenius plot discussed in Section 2.5 above.

In order to use an Arrhenius plot, samples were required to be tested at different temperatures. Each individual sample section was tested at a constant temperature. The testing temperatures were in the range of 60°C to 200°C.

A moisture test took roughly 43 minutes (2600 seconds). Moisture was introduced into the chamber at specific times for 100 seconds. There was then a wait period to allow the resistance of the TCO section to settle again. The times of wait periods and when moisture was introduced during the 2600 seconds can be seen in Table 3.1 below.

The temperature recorded was from the temperature sensor, this means that while the heater is at 90°C, the TCO section and glass pane it was prepared on may not yet be at a stable temperature. The initial wait of 600 seconds was to allow the glass of the TCO section to reach a stable temperature.

Moisture/Wait	Time
Wait	0 - 600
Moisture	600 - 700
Wait	700 - 1100
Moisture	1100 - 1200
Wait	1200 - 1600
Moisture	1600 - 1700
Wait	1700 - 2100
Moisture	2100 - 2200
Wait	2200 - 2600

Table 3.1: Times to introduce moisture into heating chamber and wait for TCO sample section to stabilize.

The temperature was set in the LabView VI seen in Figure 3.12 below. This VI also allows the run time of the experiment, type of measurement (resistance vs time), applied voltage across the circuit in series and known resistor value to be set. The resistance values were recorded in a .dat file to a folder specified in the VI. This is 'Sample Name' in Figure 3.12 below. The elapsed time indicates when moisture should be introduced into the system. When the time reaches 600 seconds, the nebulizer is turned on. Once the time is 700 seconds, the nebulizer is turned off and this is repeated with respect to Table 3.1 above.

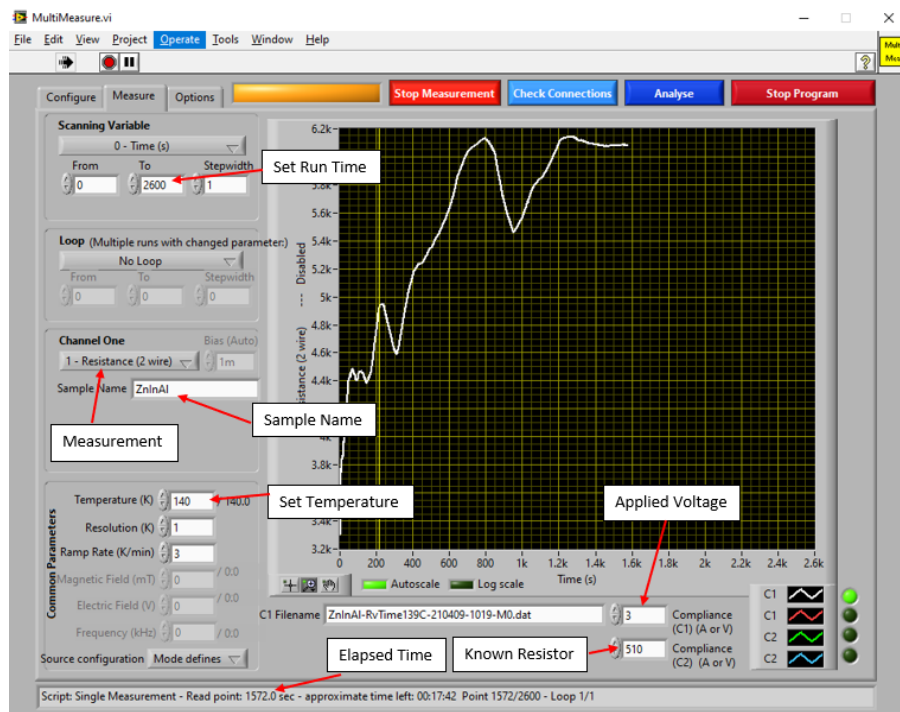


Figure 3.12: LabView VI used to set up and run moisture tests.

3.4.1 Activation Levels

In order to obtain the activation energy (E_a) of TCO samples due to moisture, an Arrhenius plot was used. To obtain an Arrhenius plot, the change in resistance of a TCO sample for multiple temperatures was required.

The following steps were followed for all TCO samples to obtain E_a for each:

1. Obtain the resistance value of the TCO sample section when the nebulizer is turned on, introducing moisture into the heating chamber, and when it is turned off.
2. Subtract the resistance value before the moisture is introduced from the resistance value after the moisture is introduced and divide by the time the nebulizer was turned on (100 seconds) to obtain the slope of the change in resistance.
3. Repeat for all times moisture was introduced into the heating chamber and obtain the average slope value.
4. Repeat this process for all TCO sample sections at different temperatures.
5. Create a graph of $\ln(\text{Slope})$ vs. $1/\text{Temperature}$ and fit a best fit line to the data.
6. The slope of the best fit line is equal to $-\frac{E_a}{k_B}$.

4 Results & Discussion

4.1 I-V Graph of device

I-V graphs were created to test the Ohmic properties of the PCIe device. Two I-V curves were created, the first had a known resistor directly connected into the breadboard in place of a TCO sample section and the second had a known resistor connected through the connection clips. This was to ensure the device and connection clips were Ohmic and to observe if the connection clips altered the resistance value recorded.

Within the circuit in series, the known resistor was 510Ω and the known resistor in place of the TCO sample section was $1.49k\Omega$. Due to the resistors being in series, the total resistance of the circuit is $2k\Omega$. There may have also been additional resistance from the wires used within the circuit, however, this was negligible in comparison to the two known resistors.

4.1.1 Direct Connection

Figure 4.1 below displays the I-V graph created with a known resistor directly connected into the circuit in place of a TCO sample section.

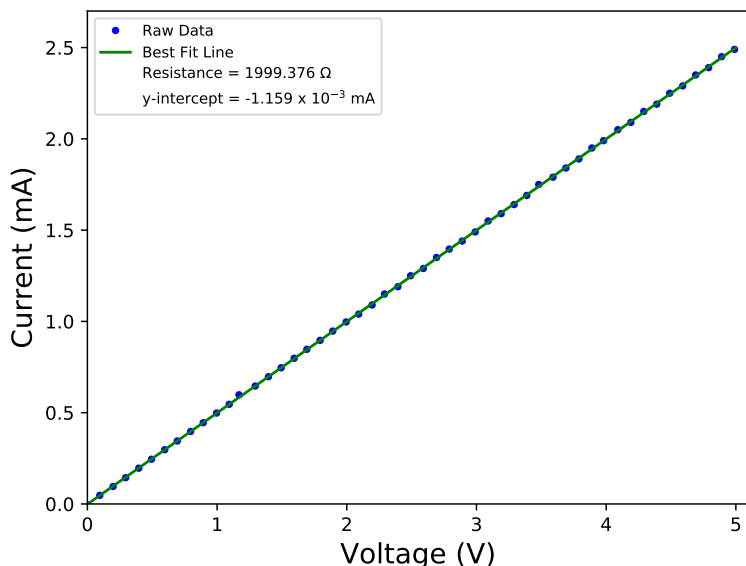


Figure 4.1: I-V Graph of PCIe device with resistor connected in breadboard in place of TCO sample section.

The graph displays a straight line with an inverse slope value of 1999.376Ω . The best fit line intercepts the y-axis at -1.59×10^{-3} mA. While the straight line of this I-V curve does not pass through the origin, it can still be said that it is Ohmic. The difference between the y-intercept value and origin is in the order of 10^{-3} mA, this is negligibly small. The inverse slope value is very close to the total resistance value of the circuit with a difference of 0.624Ω (0.03%)

4.1.2 Connection Through Clips

Figure 4.2 below displays the I-V graph created with a known resistor connected through the connection clips in place of a TCO sample section.

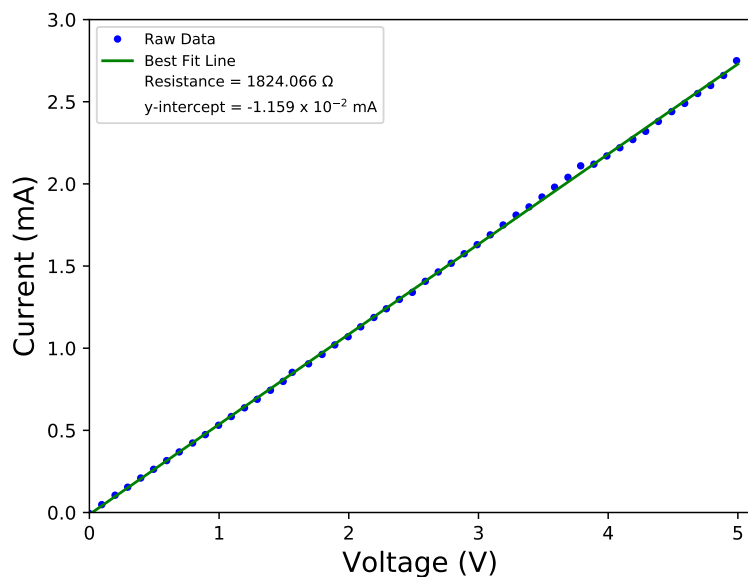


Figure 4.2: I-V Graph of PCIe device with resistor connected through clips in place of TCO sample.

The graph displays a straight line with an inverse slope value of 1824.066Ω . The best fit line intercepts the y-axis at -1.159×10^{-2} mA. While the straight line of this I-V curve does not pass through the origin, it can still be said that it is Ohmic. The difference between the y-intercept value and origin is in the order of 10^{-2} mA, this is negligibly small. The inverse slope value has an error of 175.934Ω (8.79%) with respect to the total resistance of the circuit.

While this resistance value is incorrect, this project is concerned with the change in resistance, not the absolute value. This means that if the difference between the absolute resistance value and recorded resistance value is constant, this is acceptable.

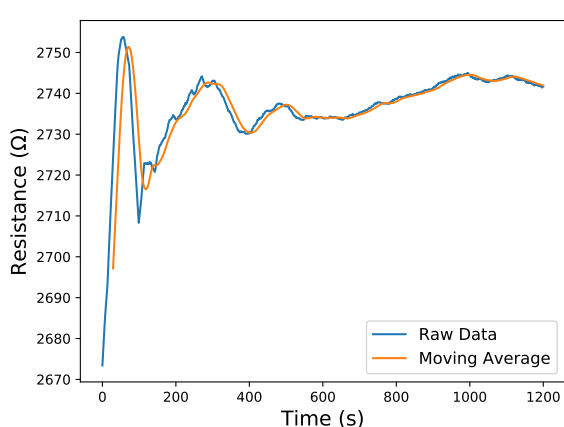
Straight line graphs can be observed in Figure 4.1 and Figure 4.2. This means that the PCIe device and connection clips are both Ohmic. An error in recorded resistance can be seen from the connection clips, however this is acceptable. Since the PCIe device and connection clips are both Ohmic, any non-Ohmic occurrences in measurements must be due to the TCO sample section being tested.

4.2 Resistance Change

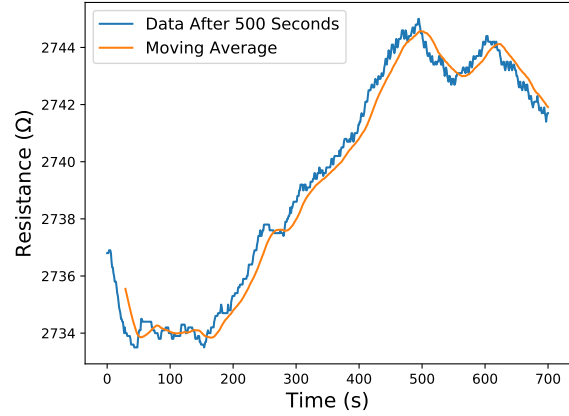
While this project is focused on the change in resistance and not the absolute resistance value, it was important to understand how the resistance of a TCO sample section deviated while it was heated. To achieve this, two graphs were made, the first while a TCO sample section was under Nitrogen flow and the second when the heating chamber was open so that the TCO sample section was exposed to Oxygen. During both tests, a TCO sample section was heated to 70°C degrees and the resistance was recorded for 20 minutes.

4.2.1 Nitrogen Flow

Figure 4.3a displays the resistance of a TCO sample section under Nitrogen flow for 1200 seconds. Initially, there is a large change of resistance. This can be attributed to the TCO sample section and glass pane continuing to reach the set temperature of 70°C. When the set temperature value is reached by the heater, recording of resistance values is commenced. While the heater is at 70°C, the TCO sample section and glass pane may not be. This means that the initial fluctuation in resistance is due to the TCO sample section and glass pane continuing to reach the desired temperature.



(a) Resistance of TCO sample section at 70°C under Nitrogen flow and moving average of data.



(b) Resistance of TCO sample section at 70°C under Nitrogen flow and moving average of data after 500 seconds.

Figure 4.3: Resistance of TCO sample section at 70°C under Nitrogen flow and moving average of data.

The initial fluctuation of resistance begins to settle after 500 seconds, as the TCO sample section and glass pane finally reached 70°C. Figure 4.3b displays the resistance of a TCO sample section under Nitrogen flow after the first 500 seconds. By removing the initial 500 seconds, any change in resistance seen must be due to the TCO sample section and PCIe device and not because the TCO sample section and glass pane is still heating up.

Table 4.1 below displays the maximum, minimum and difference in resistance recorded after the initial 500 seconds for both the raw data and moving average.

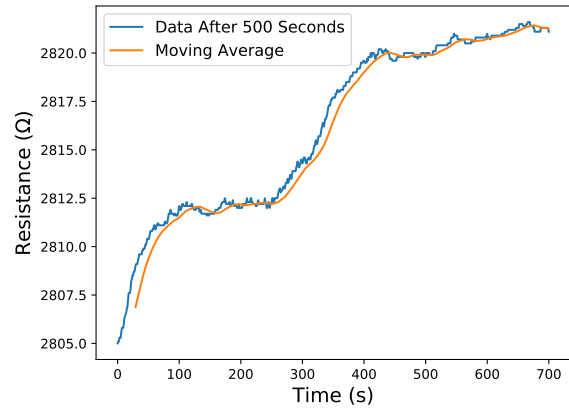
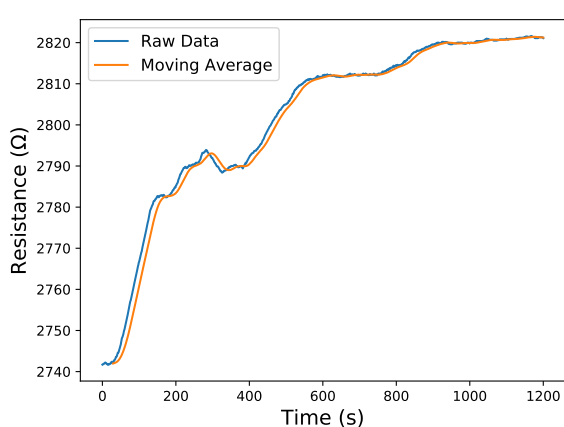
Resistance	Raw Data	Moving Average
Max (Ω)	2745	2744.57
Min (Ω)	2733.5	2733.84
Difference (Ω)	11.5	10.73

Table 4.1: Maximum, minimum and difference in resistance values of TCO sample section under Nitrogen flow at 70°C.

The difference in resistance of the raw data is 11.5Ω and 10.73Ω for the moving average. To improve this difference, the experiment could be carried out for a longer time to allow the resistance value to level out further. However, this difference is a good starting point as it is 0.42% of the average resistance value between the maximum and minimum resistance values.

4.2.2 Oxygen Exposure

Similar to Figure 4.3a above, Figure 4.4a below displays the resistance of a TCO sample section at 70°C and the moving average of the data. For this experiment, the chamber was open to air, exposing the TCO sample section to Oxygen. There is an initial increase in resistance due to the TCO sample section and glass pane continuing to reach 70°C. Figure 4.4b below displays the change in resistance after 500 seconds. Similar to Figure 4.3b, the TCO sample section continues to experience fluctuations resistance.



(a) Resistance of TCO sample section at 70°C exposed to Oxygen and moving average of data. (b) Resistance of TCO sample section at 70°C exposed to Oxygen and moving average of data after 500 seconds.

Figure 4.4: Resistance of TCO sample section at 70°C exposed to Oxygen and moving average of data.

The maximum, minimum and difference in resistance is displayed in Table 4.2 below. The difference in resistance of the raw data is 16.6Ω and 14.56Ω for the moving average. The difference in resistance is 0.59% of the average resistance value between the maximum and minimum resistance values.

Resistance	Raw Data	Moving Average
Max (Ω)	2821.6	2821.43
Min (Ω)	2805	2806.87
Difference (Ω)	16.6	14.56

Table 4.2: Maximum, minimum and difference in resistance values of TCO sample section exposed to Oxygen at 70°C .

It is difficult to compare these measured values to the absolute value of the TCO sample section. It was observed in Figure 4.2 from Section 4.1.2 above that the resistance recorded using the connection clips is incorrect. This error in measurement may be increased by heating the clips to 70°C . However, since the difference of resistance recorded in comparison to the average recorded after 500 seconds was 0.42% and 0.59% under Nitrogen flow and exposed to Oxygen, respectively, the deviation is acceptable for measurements focused on the change in resistance.

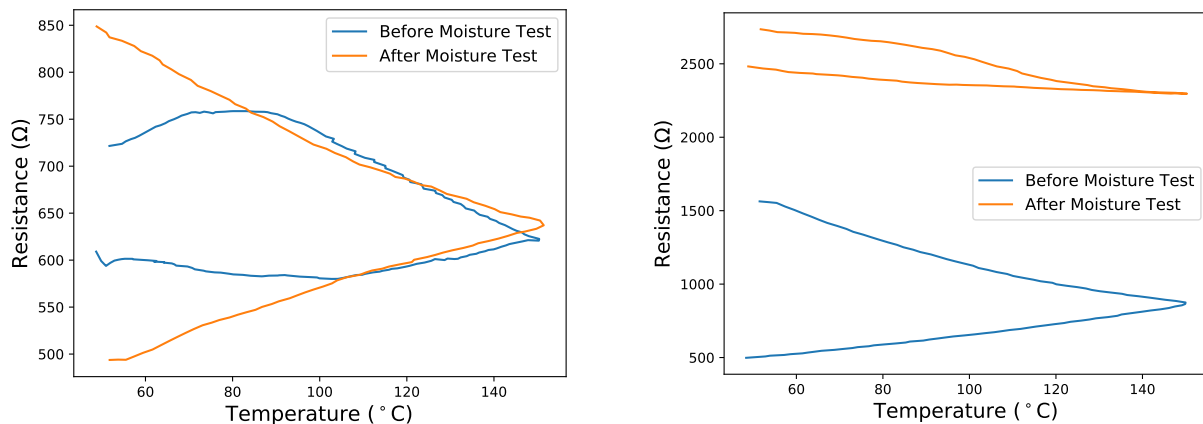
4.3 Accelerated Ageing Comparison

In order to examine the change in the working condition of TCO samples after moisture tests and degradation has occurred, round-trip tests were carried out. These tests were completed under constant Nitrogen flow. Resistance change of TCO sample sections were recorded while being heated from 50°C to 150°C and back to °C.

This round-trip test was completed immediately before and after a moisture test. This ensured that any resistance measurement discrepancies were minimal. Discrepancies could have arisen if the TCO sample section was removed to be tested at a later time. This would result in a different connection between the TCO sample section and connection clips being made.

4.3.1 Sample ZnO:In

Figure 4.5a below displays the round-trip tests of a ZnO:In sample section before and after a moisture test at 70°C was completed. It is clear that the moisture test at 70°C did not greatly affect the sample section. The working resistance of the sample section has not increased. There is a difference in resistance at lower temperatures which may be due to the Nitrogen affecting the sample section and possibly improving the working condition during the moisture and round-trip tests.



(a) Round-trip tests of ZnO:In sample section before and after moisture test at 70°C
(b) Round-trip tests of ZnO:In sample section before and after moisture test at 200°C

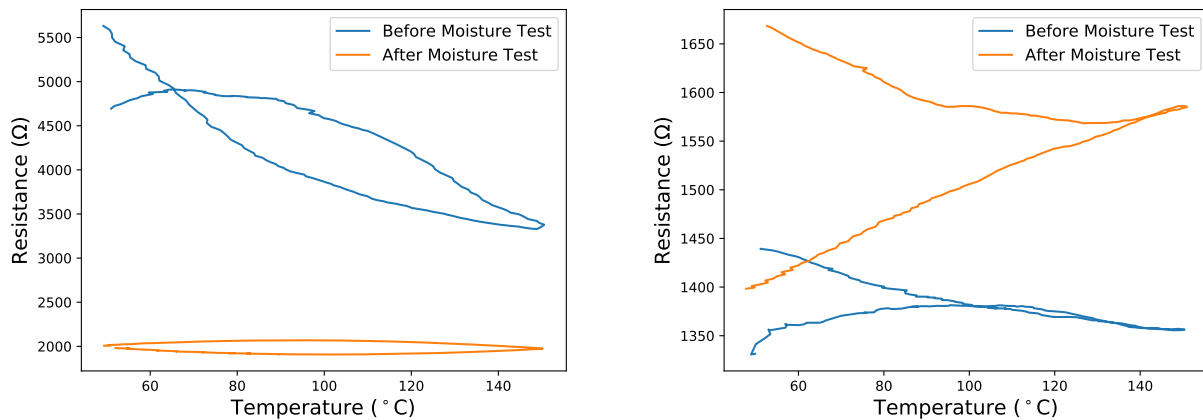
Figure 4.5: Round-trip tests of ZnO:In sample sections before and after moisture tests at 60°C and 200°C.

Figure 4.5b above displays the round-trip tests of a ZnO:In sample section before and after a moisture test at 200°C was completed. The graph displays a significant increase in working resistance of the sample section. The resistance has increased by roughly 1.5kΩ. This means that the moisture test at 200°C affected the sample section. This was expected.

4.3.2 Sample ZnO:InAl

Figure 4.6a below displays the round-trip tests of a ZnO:InAl sample section before and after a moisture test at 60°C was completed. The round-trip after the moisture test was carried out displays a lower and improved resistance values. This highlights the importance of sufficiently annealing an old TCO sample section before carrying out tests.

The ZnO:InAl sample was fabricated over a year before testing took place. This means that the working condition of the TCO sample section was improved while it was under Nitrogen flow during the round-trip tests and moisture test while the moisture test at 60°C was insufficient to degrade the working condition of the sample section.



(a) Round-trip tests of ZnO:InAl sample sections before and after moisture test at 60°C (b) Round-trip tests of ZnO:InAl sample section before and after moisture test at 200°C

Figure 4.6: Round-trip tests of ZnO:InAl sample sections before and after moisture tests at 60°C and 200°C.

Figure 4.6b above displays the round-trip tests of a ZnO:InAl sample section before and after a moisture test at 200°C was completed. The graph displays an increase in working resistance after the moisture test was carried out. This means that the working condition of the sample section was degraded during the moisture test.

The resistance increased by roughly 250Ω which is a smaller increase than that experienced by the ZnO:In sample section, seen in Figure 4.5b. It was expected that moisture tests would degrade the ZnO:In sample more than the ZnO:InAl sample.

I had insufficient time to carry out round-trip tests for the amorphous samples (ZTO-86, ZTO-90) as I focused on completing moisture tests of all samples.

4.4 Activation Energy

Figure 4.7 displays the resistance change of a ZnO:InAl sample section during a moisture test at 200°C. There is an initial drop in resistance value within the first 50 seconds. This is due to the sample section and glass pane taking longer to reach 200°C. This was discussed further in Section 4.2 above. The times when moisture is introduced into the heating chamber by turning the nebulizer on are highlighted in red.

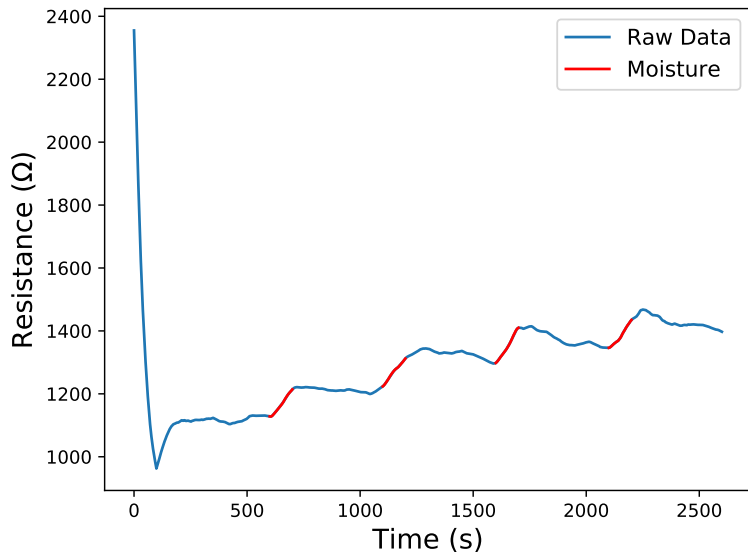


Figure 4.7: Raw data of a moisture test carried out on a ZnO:InAl sample at 200°C. Times when moisture has been introduced into the heating chamber are highlighted.

To obtain a better graph of resistance change of the sample section and the instances moisture was introduced into the heating chamber, the initial 500 seconds of the test were removed. This produced Figure 4.8 below.

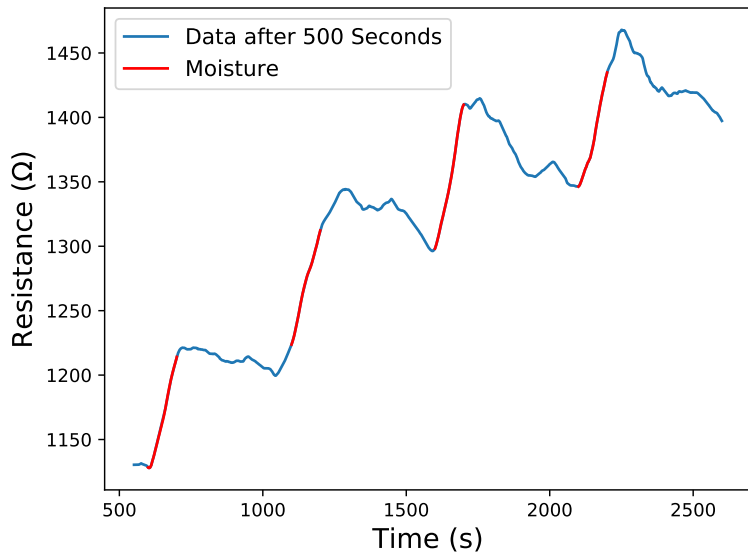


Figure 4.8: Data of a moisture test carried out on a ZnO:InAl sample at 200°C after initial 500 seconds. Times when moisture has been introduced into the heating chamber are highlighted.

From Figure 4.8 above, it is clear that the times when the resistance of the sample section changes is not limited to when the nebulizer is turned on and off. This is displayed best at the

second instance moisture is introduced. There is a change in resistance before the nebulizer is turned on. This is possibly due to the resistance value of the sample section continuing to stabilize following the first introduction of moisture into the heating chamber. An increase in resistance continues to occur when the nebulizer is turned off. While the nebulizer is turned off and no more water vapour is introduced into the heating chamber, a certain level of moisture remained in the chamber until the Nitrogen flow purges the chamber.

To reduce this change in resistance before the nebulizer is turned on, a longer wait period between moisture introduction into the chamber could be used. This would give the sample section resistance value sufficient time to stabilize. A humidity sensor could be used to understand the RH level within the heating chamber after the nebulizer is turned off. While the nebulizer is turned off, there may still be enough moisture within the chamber to affect the sample section.

As previously detailed in Section 2.3, Figure 2.3 and Figure 2.4, *Yaklin et al.* proved that ageing of a TCO sample can occur at high temperatures with low RH levels. [16] From this finding, it can be said that a sufficient RH level to degrade the sample section will remain in the heating chamber for some time after the nebulizer is turned off. Due to this, the resistance change of the sample section after the nebulizer is turned off could be included in the calculations to obtain the activation level. The amount of extra time included would depend on the testing temperature and rate the RH level decreases.

The rate at which residual moisture is removed from the heating chamber after the nebulizer is turned off is dependent on the flow rate of Nitrogen. A high flow rate would remove moisture and decrease the RH level faster than a low flow rate. In order to keep the flow rate constant throughout all moisture tests, a flow meter could be added to the system. For this project, the Nitrogen flow was kept low. However, there was no way to ensure the flow rate was equal throughout testing.

Temperature (K)	Average Slope (Ω/s)
333.15	0.054
343.15	0.09675
353.15	0.0515
363.15	0.135
373.15	0.238
393.15	0.4195
413.15	0.286
453.15	0.7085
473.15	0.936

Table 4.3: Average slope of ZnO:InAl sample for increasing temperatures.

The average slope of the change in resistance of the ZnO:InAl sample sections while moisture is introduced into the heating chamber for a range of temperatures is displayed in Table 4.3 above. There were some instances in lower temperatures when moisture introduction into the heating chamber resulted in a reduction in resistance of the sample section. This was possibly due to the moisture cooling down the sample section. These occurrences were not included in calculations for the average slope.

Figure 4.9 below displays an Arrhenius plot of $\ln(\text{Slope})$ against $1/\text{Temperature}$ for the ZnO:InAl sample. A best fit line of the data was added.

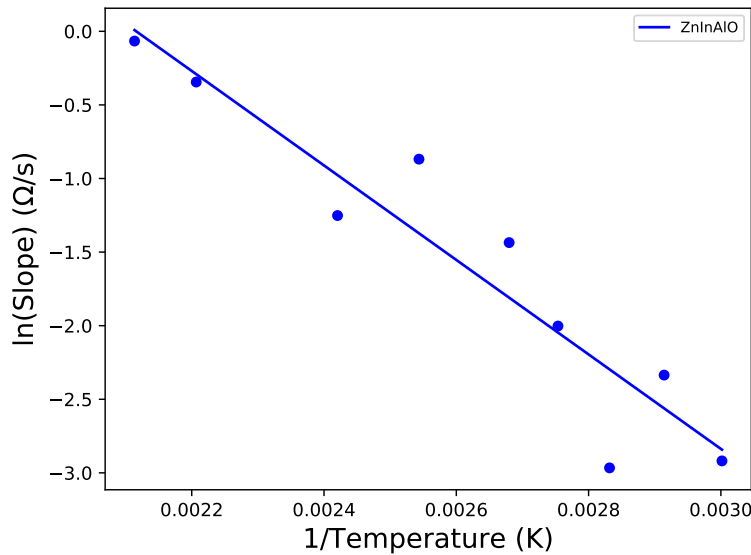


Figure 4.9: Arrhenius plot for ZnO:InAl sample.

The procedure followed to obtain the Arrhenius plot for the ZnO:InAl sample seen in Figure 4.9 above was repeated for the remaining samples, ZnO:In, ZTO-86 and ZTO-90. The Arrhenius plots of each can be seen in Figure 4.10 below. Data used to create this graph can be found in Appendix B.

From Figure 4.10 below, it is clear that ZnO:In experienced the highest level of degradation during the moisture tests. This was expected as the doping of In causes structural weaknesses in the crystal lattice of ZnO. ZnO:InAl experienced the second highest level of degradation during the moisture tests. While In causes structural weaknesses in the crystal lattice of ZnO, a combination of In and Al doping reduces these structural weaknesses.

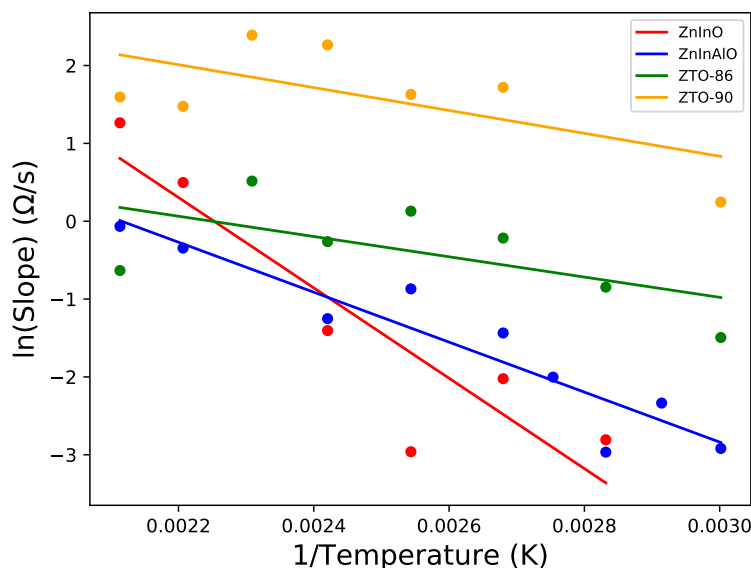


Figure 4.10: Arrhenius plot for all TCO samples.

ZTO-90 was showed the second best resilience to degradation from moisture tests, while ZTO-86 showed the best resilience. It was expected that the amorphous ZTO samples would degrade

less than the doped ZnO samples. The difference in stability under moisture between the amorphous ZTO samples is due to slight structural differences and different thickness. [18]

TCO Sample	Slope	E_a J/mol
ZnO:InAl	-3209.51	386.04
ZnO:In	-5804.07	698.12
ZTO-86	-1302.46	156.66
ZTO-90	-1469.42	176.74

Table 4.4: Slopes of best fit lines for all TCO samples and calculated activation energy, E_a .

Table 4.4 above displays the slopes of the best fit lines of the TCO samples and the corresponding activation energy, E_a . ZTO-86 has the lowest activation energy of 156.66 J/mol while ZnO:In has the highest activation energy of 698.12 J/mol.

Due to ZnO:In having the highest activation, it is the most sensitive to temperature change. Of the four TCO samples tests, ZTO-86 is the least sensitive to temperature change. However, this does not mean that ZTO-86 is a reliable replacement for ITO. ZTO-86 was fabricated on a substrate at 450°C, which is still far too high. In order for a TCO to be used in place of ITO, it must be fabricated under 200°C.

5 Conclusions & Future Prospectives

5.1 Conclusions

This project has produced a device capable of measuring the resistance change of ZnO:In, ZnO:InAl and ZTO samples within a heating chamber. By recording the change of these samples in a high-humidity environment, an Arrhenius plot and the activation energy of each was found.

It was seen that ZTO is more stable in high-humidity environments than Zn:InAl, which is more stable than Zn:InO. The ZTO samples tested are less sensitive to temperature change within a high-humidity environment than the doped ZnO samples. Activation energies for the ZTO-86 and ZTO-90 were found to be 156.66 J/mol and 176.74 J/mol, respectively. These are lower activation energies than those found for Zn:InAl and Zn:In which were found to be 386.04 J/mol and 698.12J/mol, respectively.

While it is clear that amorphous ZTO is more stable in high-humidity environments than doped ZnO, all samples tested during this project were fabricated through spray pyrolysis on substrates exceeding 400°C. In order to replace ITO as the leading TCO used in optoelectronic devices, amorphous ZTO and doped Zinc oxide must be grown in temperatures under 200°C and remain stable. In light of this, new forms of ZnO TCOs must be constantly developed.

The aims of this project was to build a device capable of measuring the resistance change of TCO samples in a high-humidity environment and to compare the stability of amorphous ZTO and doped ZnO:InAl and ZnO:In. As both of these aims have been achieved, this project is deemed successful.

5.2 Future Prospectives

This project has shown that amorphous ZTO is more stable in high-humidity environments than doped ZnO. However, as new forms of both are constantly being developed with new precursors, fabrication methods and substrate growth temperatures, the stability should be constantly tested.

Further developments could be made to the PCIe device, connection clips and heating chamber. These developments could reduce errors involved in measurements and give a better understanding to the stability of ZnO in high-humidity environments and how to improve it. A humidity sensor attached to the heating chamber would give an insight into the RH level experienced by a TCO sample throughout testing. This would positively affect both data recorded and final results. The connection clips need to be improved as the pressure from the clip on a TCO sample was not constant throughout testing. This drastically affects the resistance recorded. This would also be a step toward a device capable of recording the absolute value of a TCO sample, not just the change in resistance. This would be a great improvement as errors in measurement could be better represented. As the transparency of the ZTO samples was previously measured, obtaining a similar graph of transparency vs. wavelength would be beneficial in understanding how moisture tests degrade the structure of the TCOs.

As the requirement for clean and renewable energy is increasing throughout the world, it is vital that robust and long lasting solar cells are fabricated. As many solar cells utilise TCOs to improve their energy conversion rate, stable and efficient TCO thin films need to be constantly developed and improved.

5.3 A Brief note on Covid-19

This project was commenced and completed during the Covid-19 pandemic. Due to this, some goals of the original project brief were not achieved.

A lot of work was completed during the first semester of this college year. The PCIe device had been built and programmed to record the resistance of one TCO sample. It was hoped that during the second semester, there would be sufficient time to test TCO samples with this device before further developing it to record multiple TCO samples at once. This would have been beneficial to save time and also help in the comparison of different TCO samples. Testing of TCO sample transparency before and after degradation was also discussed as a possible goal to be achieved during this project.

Due to the lockdown during the start of 2021, DCU Glasnevin campus was closed and there was no access to labs. Once this lockdown had eased and students were given access to labs, I had 5 weeks to become accustomed to testing the TCO samples. This was a very short amount of time to obtain relevant data and retest certain samples. There was a discussion to bring the equipment home and conduct tests there. While that would have provided me with sufficient time to gather data, I had no Nitrogen supply. A Nitrogen supply during my testing was vital in order to reduce Oxygen and moisture levels in the heating chamber. Without a Nitrogen flow, the data obtained would not be as definitive as presented in this report.

References

- [1] Hartnagel HL, Dawar AL, Jain AK, Jagadish C. Semiconducting Transparent Thin Films. Institute of Physics Publishing, Techno House, Redcliffe Way, Bristol, UK: IOP Publishing Ltd.; 1995. Chapter 1, Transparent Conducting Oxides: Basic Properties p. 1-20.
- [2] Stadler A. Transparent Conducting Oxides-An Up-To-Date Overview. 2012 Apr 19;5(12):661-83.
- [3] Janotti A, Van De Walle CG. Fundamentals of zinc oxide as a semiconductor. Reports Prog Phys. 2009;72(12).
- [4] Minami T, Kuboi T, Miyata T, Ohtani Y. Stability in a high humidity environment of TCO thin films deposited at low temperatures. physica status solidi (a) 2008;205(2):255-60.
- [5] Minami T. Present status of transparent conducting oxide thin-film development for Indium-Tin-Oxide (ITO) substitutes. Thin Solid Films. 2008;516(17):5822-8.
- [6] Hartnagel HL, Dawar AL, Jain AK, Jagadish C. Semiconducting Transparent Thin Films. Institute of Physics Publishing, Techno House, Redcliffe Way, Bristol, UK: IOP Publishing Ltd.; 1995. Chapter 5, Applications of Transparent Conducting Oxide Films p. 306-354.
- [7] Sundaramoorthy R, Pern FJ, DeHart C, Gennett T, Meng FY, Contreras M, et al. Stability of TCO window layers for thin-film CIGS solar cells upon damp heat exposures: part II. Reliab Photovolt Cells, Modul Components, Syst II. 2009;7412:74120J.
- [8] CastaÃ±eda L, Maldonado A, Escobedo-Morales A, AvendaÃ±o-Alejo M, GÃ¶mez H, Vega-PÃ¡rez J, et al.. Indium doped zinc oxide thin films deposited by ultrasonic spray pyrolysis technique: Effect of the substrate temperature on the physical properties. Materials Science in Semiconductor Processing 2011;14(2):114-9.
- [9] Jayaraman VK, Alvarez AM, Bizarro M, Koudriavtsev Y, Amador MDLLO. Effect of precursor type and doping concentration on the physical properties of ultrasonically sprayed aluminium and indium co-doped zinc oxide thin films. Thin Solid Films 2017;642:14-9.
- [10] Hegazy AR, Salameh B, Alsmadi AM. Optical transitions and photoluminescence of fluorine-doped zinc tin oxide thin films prepared by ultrasonic spray pyrolysis. Ceramics International 2019;45(15):19473-80.
- [11] Jagadish C, Pearton SJ. Zinc Oxide Bulk, Thin Films and Nanostructures. The Boulevard, Langford Lane, Kidlington, Oxford, UK : Elsevier Ltd.; 2006. Chapter 1, Basic Properties and Applications of ZnO; p. 1-20.
- [12] Vaseem M, Umar A, Hahn Y-B. ZnO Nanoparticles: Growth, Properties, and Applications. Vol. 5, Metal Oxide Nanostructures and Their Applications. 1988. 1-36 p.
- [13] Naoi K, Nagano Y, Naoi W. Transparent Conductors - A Status Review. Thin Solid Films. 2013;102(256):1-3.
- [14] Hartnagel HL, Dawar AL, Jain AK, Jagadish C. Semiconducting Transparent Thin Films. Institute of Physics Publishing, Techno House, Redcliffe Way, Bristol, GB: IOP Publishing Ltd.; 1995. Chapter 2, Growth Techniques: p. 22-133.
- [15] Perednis D, Gauckler LJ. Thin film deposition using spray pyrolysis. J Electroceramics. 2005;14(2):103-11.

- [16] Yaklin MA, Schneide DA, Norman K, Granata JE, Staiger CL. Impacts of humidity and temperature on the performance of transparent conducting zinc oxide. In: Conference Record of the IEEE Photovoltaic Specialists Conference. 2010. p. 2493-6.
- [17] Pern FJ, Noufi R, To B, DeHart C, Li X, Glick SH. Degradation of ZnO-based window layers for thin-film CIGS by accelerated stress exposures. In: Reliability of Photovoltaic Cells, Modules, Components, and Systems. SPIE; 2008. p. 70480P.
- [18] Zhussupbekova, A., Caffrey, D., Zhussupbekov, K., Smith, C. M., Shvets, I. V., & Fleischer, K. (2020). Low-Cost, High-Performance Spray Pyrolysis-Grown Amorphous Zinc Tin Oxide: The Challenge of a Complex Growth Process. ACS Applied Materials & Interfaces, 12(41), 46892-46899.
- [19] The Arrhenius Law- Activation Energies [Internet]. 2020 [cited 2021 Apr 12]. Available from: <https://chem.libretexts.org/@go/page/1444>
- [20] Method, F. P., State, S., Virtual, P., Sciences, P., Vishwa, A., & Virtual, V. (2015). Resistivity by Four Probe Method. 6â€¢7.
- [21] Probe, F., & The, M. (2013). Module-2 : Two probe and four probe methods- van der Pauw method. D, 08.

A Appendix: Risk Assessment

Title Hazard Identification & Risk Assessment				Prepared by:				
School/Unit/Faculty name:	School of Physical Sciences			Philip Keenan				
Groups affected:	Staff Student							
Hazards	Is the Hazard present? Y/N	What is the risk?	Controls - Controls in place to reduce risks			Is the control in place? Y/N	Likelihood	Severity
								Risk Rating (L x S)
								L/M/H
Physical - High Temperature	Y	A heating module used is capable of reaching 400°C.	The program that controls the heater has a default temperature of 15°C so when the program is not in use, the heater is set to this temperature.			Y	2	1
Physical - Covid-19	Y	Possibility of catching Covid-19.	Wear a face mask at all time, sanitize hands entering and leaving the building, sanitize desk before and after use, comply with contract tracing measures in place.			Y	2	2
Physical - Electric Shock	Y	Risk of receiving a shock from plugs and pin terminal	Only have necessary devices plugged in, do not have pin terminal plugged in while attaching wires.			Y	1	1
Physical - Ergonomics	Y	Risk of eye strain and back problems from looking at a screen and sitting for too long.	Stand up from time to time, adjust height of monitor to the correct height, go for walks/breaks at reasonable intervals.			Y	1	1
Physical - Nitrogen Gas	Y	Risk of inhaling large amounts of Nitrogen gas. This could cause physical and mental damages.	Insure all tubes are connected before turning Nitrogen gas supply on. Only use small flow of Nitrogen. Extractor fan is constantly on.			1	1	1

Figure A.1: Risk assessment of lab project was carried out in.

B Arrhenius Plot Data

ZnO:In Sample

Temperature (K)	Average Slope (Ω/s)
353.15	0.06035
373.15	0.1323
393.15	0.05175
413.15	0.2455
453.15	1.6441
473.15	3.541

Table B.1: Average slope of ZnO:In sample for increasing temperatures.

ZTO-86 Sample

Temperature (K)	Average Slope (Ω/s)
333.15	0.2245
353.15	0.429
373.15	0.8055
393.15	1.138
413.15	0.76967
433.15	1.675
473.15	0.531

Table B.2: Average slope of ZnTO-86 sample for increasing temperatures.

ZTO-90 Sample

Temperature (K)	Average Slope (Ω/s)
333.15	1.279
373.15	5.58367
393.15	5.097
413.15	9.635
433.15	10.916
453.15	4.372
473.15	4.932

Table B.3: Average slope of ZnTO-90 sample for increasing temperatures.

C LabView Program

The LabView Sub VIs created to control the PCIe device and integrated into the MultiMeasure VI can be accessed through the link below.

<https://drive.google.com/file/d/1EjnmCGZgDxtI0czQ1feAb-QU-apOFeH5/view?usp=sharing>